



HAL
open science

On the benefits of using cell quotas in addition to intracellular elemental ratios in flexible-stoichiometry Plankton functional type models. Application to the Mediterranean Sea

Melika Baklouti, Rémi Pagès, Elena Alekseenko, Arnaud Guyennon, Gérald Grégori

► To cite this version:

Melika Baklouti, Rémi Pagès, Elena Alekseenko, Arnaud Guyennon, Gérald Grégori. On the benefits of using cell quotas in addition to intracellular elemental ratios in flexible-stoichiometry Plankton functional type models. Application to the Mediterranean Sea. *Progress in Oceanography*, 2021, 197, pp.1-50. 10.1016/j.pocean.2021.102634 . hal-03323385

HAL Id: hal-03323385

<https://amu.hal.science/hal-03323385>

Submitted on 9 Sep 2021

HAL is a multi-disciplinary open access archive for the deposit and dissemination of scientific research documents, whether they are published or not. The documents may come from teaching and research institutions in France or abroad, or from public or private research centers.

L'archive ouverte pluridisciplinaire **HAL**, est destinée au dépôt et à la diffusion de documents scientifiques de niveau recherche, publiés ou non, émanant des établissements d'enseignement et de recherche français ou étrangers, des laboratoires publics ou privés.



Distributed under a Creative Commons Attribution - NonCommercial - NoDerivatives 4.0 International License

On the benefits of using cell quotas in addition to intracellular elemental ratios in flexible-stoichiometry Plankton Functional Type models. Application to the Mediterranean Sea.

M. Baklouti*¹, R. Pagès¹, E. Alekseenko², A. Guyennon³, and G. Grégori¹

¹*Aix-Marseille Université, Université de Toulon, CNRS, IRD, MIO UM 110, 13288 Marseille, France*

²*Shirshov Institute of Oceanology, Russian Academy of Sciences, Nakhimovsky Prospekt 36, 117997, Moscow, Russia*

³*Univ. Grenoble Alpes, INRAE, LESSEM, 2 rue de la Papeterie - BP 76 F-38402 St-Martin-d'Hères, France*

Abstract In the last decades, among the marine biogeochemical models, there have been an increasing number of marine Plankton Functional Type (PFT) models. Since the precursor NPZD models, the general trend has been towards the development of models that are more and more complex, either by the number of variables they include and/or by the level of detail they consider. In this respect, flexible-stoichiometry models have been an important step in the history of this class of models. Since then, additional developments have been described in the literature, and the present paper focuses on one of them, namely the introduction of abundance in addition to biomass to describe PFTs. This new feature offers an opportunity for model assessment with the increasing number of studies and datasets obtained by flow cytometry, and it provides the means to derive cell quotas (here expressed as an amount of a given biogenic element per unit cell) for each PFT of the model. Cell quotas are used, along with intracellular ratios, for the regulation of the kinetics of the different biogeochemical processes embedded in the model, and it is suggested here that their role may be decisive for the successful representation of some processes, such as, for example, mineralization by heterotrophic bacteria. Several other benefits provided by cell quotas are presented in this paper, among them the in-depth knowledge they provide on the functioning of the trophic web and on the nutritional status of organisms. Finally, the seasonal variations of the cell quotas in the PFT representing large phytoplankton can be used to explain the occurrence of the NW Mediterranean spring bloom from the internal status point of view.

Keywords: *Cell quota; Intracellular ratios; Flexible-stoichiometry; PFT biogeochemical model; Mechanistic; Coupled physical-biogeochemical model; Mediterranean Sea.*

*Corresponding author; melika.baklouti@mio.osupytheas.fr

1 Introduction

Coupled physical-biogeochemical ocean models are now widely used in the ocean sciences. They are involved in a broad range of studies of a different nature, from process studies to larger-scale or global-ocean scale studies. The former aim at explaining and/or quantifying some specific processes, often using a 0D model (e.g. Thingstad and Lignell, 1997; Flynn, 2003) or a coupled model in a 1DV configuration (e.g. Ayata et al., 2013; Gimenez et al., 2018), while the aim of the latter is to study biogeochemical cycles (e.g. Gnanadesikan et al., 2011; Stock et al., 2014), as well as the effect of physical processes (e.g. Lévy and Martin, 2013), or that of climate change through forecast climatic scenarios (e.g. Bopp et al., 2013, and references herein), on ocean biogeochemistry. Since the first Nutrient-Phytoplankton-Zooplankton (NPZ) models (e.g. Riley, 1946; Steele and Henderson, 1981), biogeochemical models have developed in various directions relative to their structure (number and nature of state variables and of the fluxes they include) or to the formulations of the biogeochemical processes they involve.

These regular developments have accompanied – and were sometimes triggered by – the increase in knowledge in the domain of marine biogeochemistry (e.g. the discovery of the major role of bacteria) as well as by the increase in feedback from experience in modelling. These developments have mainly concerned the number of state variables (i.e. food web compartments) they include: NPZD models with an additional detritus compartment were then developed (e.g. Fasham et al., 1990), followed by $N_x P_y Z_z D_d$ models with multiple size classes of a given trophic level and/or multiple nutrients (using a fixed stoichiometry), and later by Plankton Functional Type (PFT) and trait-based models regrouping plankton species according to the ecological functionality they share. More recently, diversity-based models including several tens of phytoplankton types of different physiological characteristics including sensitivity of growth to light, nutrient and temperature, have been developed (Follows and Dutkiewicz, 2011).

Another direction in which biogeochemical models have developed concerns the mathematical formulations of the internal biogeochemical fluxes. Models have generally increased in complexity in phase with the aim of (i) including more and more processes, as in the PISCES model (Aumont et al., 2003), or (ii) developing more and more mechanistic models such as ERSEM (Baretta et al., 1995), Eco3M (Baklouti et al., 2006b), BFM (Vichi et al., 2007b), or even (iii) elaborating a global theory such as the Dynamic Energy Budget (DEB) theory used in DEB models (Kooijman, 2000).

In essence, NPZ models, complex as they may be, consider a single biogenic element in which all the state variables are expressed, and use the Redfield C:N:P ratio to allow conversions and mass fluxes into biogenic elements that are not explicitly represented. Whether the model should include a flexible stoichiometry has been a question that has been widely debated in the literature over the two last decades, between authors who consider that NPZ models still constitute an important and viable research tool to deal with some clearly stated ques-

tions (e.g. Franks, 2002), others who conclude that the introduction of flexible stoichiometry is necessary to make the model able to reproduce or explain data (e.g. Christian, 2005; Ayata et al., 2013; Macias et al., 2019), still others who assert, taking into account the wide differences in the scenarios run with or without flexible stoichiometry, the need for additional experimental work (Tagliabue et al., 2011), or a last category of authors pointing out the inherent deficiencies revealed by models using Redfield ratios associated with Monod-type descriptions of resource-limited growth and predation (Flynn, 2010).

Flexible-stoichiometry models have been more and more widely used in the recent past, providing important and extensive results relative to the link between, on the one hand, plankton stoichiometry and ecosystem stoichiometry, and phytoplankton biogeography and the main biogeochemical fluxes including carbon export on the other hand (Klausmeier et al., 2008; Salihoglu et al., 2008; Weber and Deutsch, 2010; Letscher et al., 2015). Flexible stoichiometry models are also increasingly widely used to study the dynamics of biogeochemistry and that of the planktonic food web at global scale (e.g. Vichi et al., 2007a; Letscher et al., 2015) or at regional scales, such as for example at the scale of the Mediterranean basin (Lazzari et al., 2012, 2016).

In the present paper, our aim is to broaden the debate regarding the benefits of flexible stoichiometry to intracellular cell quotas, first defined by Droop (1968) for phytoplankton as "the amount of nutrient internal to the cells per total cell population". The dimensions of this variable depend on the measure of the cell population used. As a result, though now widely used, different definitions of cell quota are used, being either expressed as an absolute quantity, or as per unit cell or per unit biomass quantities (see for example the different use of quotas in Smirnov and Revkova (2002)). In order to avoid any confusion in the terminology, we will consider in this paper that cell quotas exclusively refer to the amount of a given biogenic element per unit cell, while the term intracellular ratio will be used to represent the ratio between the intracellular contents in two biogenic elements. In other words, the cell quota in a given element X among C, N, P, ... will be referred to as Q_X and expressed in $(\text{mol X}) \cdot \text{cell}^{-1}$, while the intracellular ratio X:Y between two elements X and Y (X and Y among C, N, P, ...) will be referred to as Q_{XY} and expressed in $(\text{mol X}) \cdot (\text{mol Y})^{-1}$.

In the Eco3M-MED model (Alekseenko et al., 2014; Guyennon et al., 2015; Gimenez et al., 2018; Pagès et al., 2020b), organisms are not only represented through several biogenic concentrations (thereby allowing calculation of intracellular ratios) but through abundance, which makes it possible to calculate and handle cell quotas as well. To the best of our knowledge, very few models in literature combine both these facilities. Some of them were used to model and study the growth of phytoplankton under nutrient limitation in microcosm/chemostat configurations (e.g. Burmaster, 1979; Klausmeier et al., 2004), or the dynamics of the planktonic food web in the Mediterranean Sea (MS hereafter) (Thingstad, 2005). DEB models (Kooijman, 2000) are also in the same vein, but they may become very complex as the number of biogenic

elements increases, at least if we keep full generality (e.g. Poggiale et al., 2010). This complexity can however be reduced by constraining assumptions. These models have all been used in 0D configurations to study some specific processes, but, as far as we know, none of them has been used for 3D coupled physical-biogeochemical modelling studies. In this paper, our aim is therefore to highlight the benefits of using models using intracellular quotas in addition to intracellular ratios to study the dynamics of the biogeochemistry of the MS and that of the planktonic food web using a 3D coupled physical-biogeochemical model.

The paper is therefore organized as follows: a presentation of the updated version of the Eco3M-MED model is first given, with a focus on the physiological processes involving cell quotas. The Results section follows, first dedicated to model skill assessment through the comparison of model outputs with in situ or satellite-derived data. The remainder of this section focuses on some information provided by the model outputs in terms of cell quotas and abundances, which are inaccessible to the models based on intracellular ratios. The benefits provided by the use of abundances and cell quotas in the model are then discussed in the last section before concluding.

2 Material and Methods

2.1 The biogeochemical flexible-stoichiometry model Eco3M-MED

The Eco3M-MED model has already been used in several studies (Alekseenko et al., 2014; Guyennon et al., 2015; Pagès et al., 2020b), sometimes using more complex versions, such as the one including two PFT of diazotrophs (Gimenez et al., 2016, 2018), or an additional PFT for the ctenophore *Mnemiopsis leidyi* (Alekseenko et al., 2019). Each of these versions of the Eco3M-MED model was also an opportunity to revisit some aspects of the formulation and parametrization of the processes. For example, the most recent versions include new formulations for the mineralization and chlorophyll synthesis processes, as well as a partially renewed set of parameters (Pagès et al., 2020b,a). Only the new developments of the model have been detailed in the papers published since the original version of Alekseenko et al. (2014), and there is now a need to provide an extensive presentation of the most recent version of the model since it now significantly differs from its original version.

In this section we will only focus on the main characteristics of the model, on some general options, and on some specific processes. The remainder of the model, namely the full set of equations and parameters is provided in an appendix (A).

The model encompasses six PFT, namely micro-, meso- and nanozooplankton, large and small phytoplankton, and heterotrophic bacteria. Each PFT is represented by an abundance and carbon (C), nitrogen (N) and phosphorous (P) concentrations, except phytoplankton which is also represented by a chlorophyll (CHL) concentration, and microzooplankton which is only

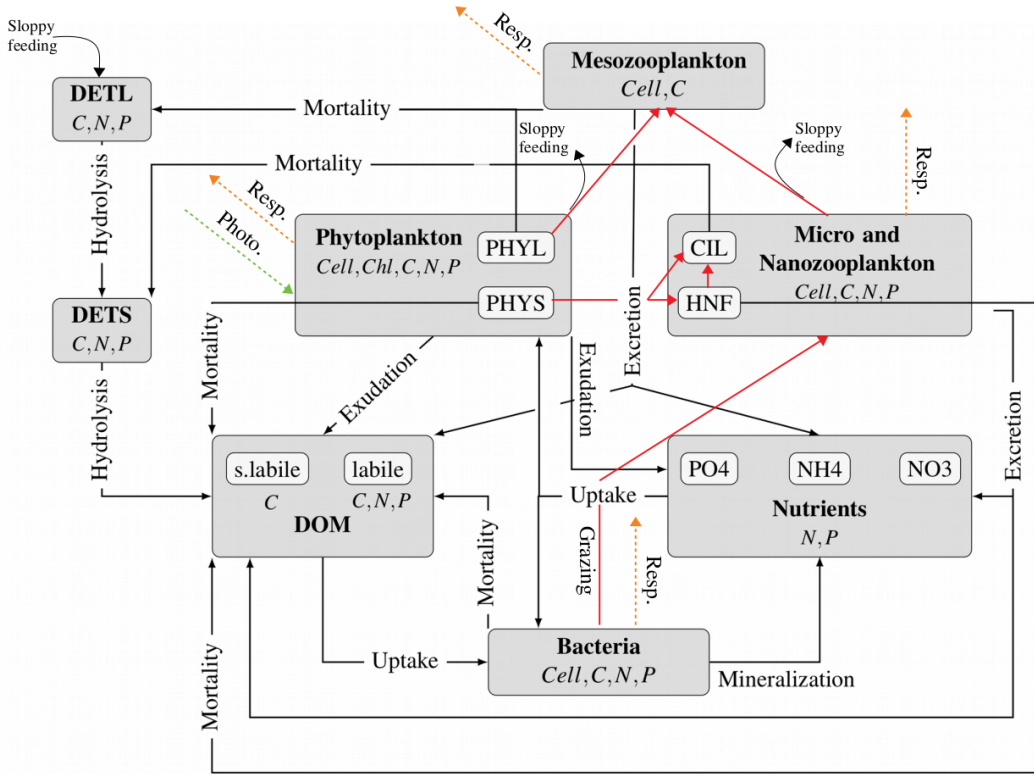


Figure 1: *Conceptual model associated with the Eco3M-MED biogeochemical model.*

expressed in terms of an abundance and a carbon concentration. Three inorganic nutrients, namely nitrate (NO_3), ammonium (NH_4) and phosphate (PO_4), as well as dissolved and particulate detrital organic material (respectively DOM and DET) are also included in the model. Only the labile pool of DOM is explicitly represented, except for the carbon pool for which semi-labile DOC is also an explicit state variable of the model. Finally, the DET compartment is split into large and small detrital particles, associated with different sinking rates. In the original version of Alekseenko et al. (2014), there was only a single DET compartment. Taking into account the splitting of the DET compartment, the conceptual model has been slightly changed. It now also includes an explicit predation of ciliates on bacteria. In short, the model now includes 37 state variables that are defined in Tab. 1 as well as their notation throughout this paper, and the associated conceptual model describing the different fluxes between state variables is given in Fig. 1.

Let X and Y represent generic biogenic elements among C, N and P, and let PFT_X be the concentration of a given PFT in element X . In each PFT, cell quotas Q_X and intracellular ratios Q_{XY} , as already defined in 1, are allowed to vary within a given range (see 2). Normalized quotas and ratios, respectively denoted \tilde{Q}_X and \tilde{Q}_{XY} , are dimensionless quotas and ratios varying

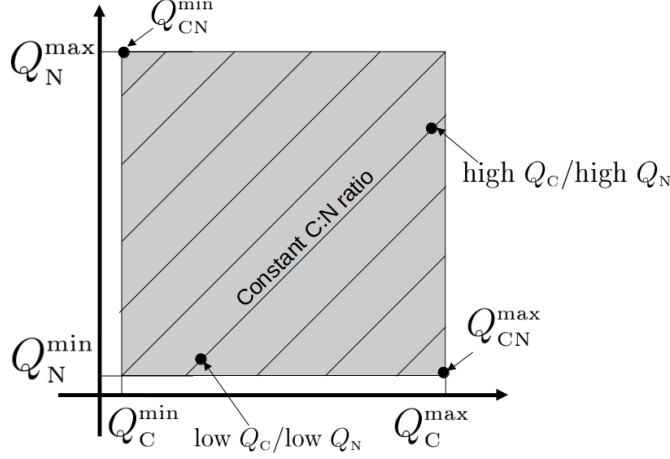


Figure 2: Variation range of quotas and ratios (grey region). For a given organism, cell quotas are bounded. As a consequence, intracellular ratios are also bounded. A given C:N ratio can be associated with a large variety of (Q_C, Q_N) couples.

between 0 and 1. They are calculated as follows:

$$\tilde{Q}_X = \frac{Q_X - Q_X^{\min}}{Q_X^{\max} - Q_X^{\min}} \quad \text{and} \quad \tilde{Q}_{XY} = \frac{Q_{XY} - Q_{XY}^{\min}}{Q_{XY}^{\max} - Q_{XY}^{\min}} \quad (1)$$

2.2 Formulation of biogeochemical processes

For most of the modelled processes, the associated rate is first controlled by cell quotas, thereby ensuring that they remain within the range $[Q_X^{\min}; Q_X^{\max}]$. Intracellular ratios are used as a second level of control to regulate the process rate in the case where the cell quota are within the authorized range $[Q_X^{\min}; Q_X^{\max}]$. This regulation is done through quota functions h_Q having generic forms similar to that given by Geider et al. (1998), and calculated either with intracellular quotas:

$$h_{Q_X} = \left(\frac{Q_X^{\max} - Q_X}{Q_X^{\max} - Q_X^{\min}} \right)^{nn} = (1 - \tilde{Q}_X)^{nn} \quad (2)$$

or with intracellular ratios:

$$h_{Q_{XY}} = \left(\frac{Q_{XY}^{\max} - Q_{XY}}{Q_{XY}^{\max} - Q_{XY}^{\min}} \right)^{nn} = (1 - \tilde{Q}_{XY})^{nn} \quad (3)$$

These functions are bounded by 0 and 1 and nn equals 0.06 (as in Geider et al. (1998)), unless stated otherwise.

2.2.1 Gross and net inflows for absorption and grazing

Let us consider the inflow F_{in} associated with a given process occurring at the specific rate r_X and involving a given biogenic element X, and a given PFT. Depending on the PFT's

intracellular status, only a fraction of this inflow (i.e. the net inflow F_{net}) will be actually retained by the PFT, the remainder being released as an outflow F_{out} . This feedback regulation is based on the quota functions defined by Eqs. 2 and 3, and the different fluxes are calculated as follows:

$$F_{in} = r_X \cdot \text{PFT}_X \quad (4)$$

$$F_{out} = r_X \cdot \text{PFT}_X \cdot (1 - h_{Q_X}^{\text{PFT}}) \quad (5)$$

$$F_{net} = F_{in} - F_{out} = r_X \cdot \text{PFT}_X \cdot h_{Q_X}^{\text{PFT}} \quad (6)$$

In the same way, the outflow (and the net flux) can also be calculated with intracellular ratios:

$$F_{out} = r_X \cdot \text{PFT}_X \cdot (1 - h_{Q_{XY}}^{\text{PFT}}) \quad (7)$$

In Eqs. 4 to 7 PFT_X stands for the PFT biomass expressed in $(\text{mol X}) \cdot l^{-1}$.

These functions are used for the regulation of the uptake of nutrients and dissolved organic matter by phytoplankton and bacteria, and for the regulation of the excess carbon and the associated DOC exudation flux when photosynthesis takes place more rapidly than is required to supply the needs of growth. They are also used to calculate the net grazing fluxes and the associated output fluxes that take the form of DOC, ammonium and phosphate excretion fluxes for all the zooplankton, and the production of faecal pellets for mesozooplankton only.

In practice, the net inflow and the outflow are calculated as follows for N and P: if $(Q_X^{\text{PFT}} \leq Q_X^{\text{PFT,min}})$ or $(Q_X^{\text{PFT}} \geq Q_X^{\text{PFT,max}})$, F_{net} and F_{out} are respectively given by Eqs. 6 and 5, otherwise, F_{net} and F_{out} are calculated in the same way but with the X:C ratio (Q_{XC}^{PFT}) used instead of the X quota in the calculation of $h_{Q_X}^{\text{PFT}}$. The maximum (or the minimum according to the regulation) between the two F_{out} fluxes is then used. DOC exudation and corresponding fluxes are detailed in (A.2).

2.2.2 Mineralization by heterotrophic bacteria

This process is first represented through a classical uptake of dissolved organic matter which allows the calculation of the outflow using Eq. 5. Non-zero outflows are either redirected to the dissolved organic matter, or to a mineral compartment (NH_4 or PO_4) in the case of mineralization. The distribution of the outflow between those two possible directions is controlled by the carbon intracellular quota Q_C for bacteria, based on the underlying assumption that, the more bacteria are carbon-limited, the more they will proceed to DOM mineralization in order to extract carbon from it (see also the Discussion section dealing with the formulation of this process). The flux of remineralized dissolved organic matter F_{rem} is then calculated as follows:

$$F_{rem} = h_{Q_C}^{\text{BAC}} \cdot F_{out}, \quad (8)$$

while the remaining outflow turns back to the DOM compartment.

2.2.3 Chlorophyll synthesis

The previous chlorophyll synthesis formulation used in Eco3M-MED was similar to that of Geider et al. (1998), except that the feedback regulation by phytoplankton used a Chl:N ratio instead of the N:C ratio of the original formulation (see Baklouti et al. (2006a) for more details). The new version implemented is still in the same vein, but with a feedback regulation involving the carbon quota. The specific rate of chlorophyll synthesis then writes:

$$f^{\text{PChl}} = \rho_{\text{CHL}} \cdot f_{\text{PHY}}^{\text{upt}_N} \cdot \left(\frac{Q_{\text{C}}^{\text{PHY,max}} - Q_{\text{C}}^{\text{PHY}}}{Q_{\text{C}}^{\text{PHY,max}} - Q_{\text{C}}^{\text{PHY,min}}} \right)^{\text{nphy}} \cdot \left(\frac{\theta_N^{\text{max}} - \theta_N}{\theta_N^{\text{max}} - 0.42} \right)^{\text{nchl}} \quad (9)$$

where,

$$\rho_{\text{CHL}} = \theta_N^{\text{max}} \frac{f^{\text{PP}}}{\bar{a}^* \phi_{\text{C}}^{\text{max}} \theta E} \quad \theta = \frac{\text{PHY}_{\text{CHL}}}{\text{PHY}_{\text{C}}} \quad f^{\text{PP}} = f_{nr}^{\text{PP}} \cdot h_{Q_{\text{C}}}^{\text{PHY}} \quad (10)$$

In Eq. 9, ρ_{CHL} stands for the ratio between the effective and the maximum primary production rates, $f_{\text{PHY}}^{\text{upt}_N}$ refers to the gross cumulative (i.e. from all nitrogen sources) N uptake rate (see Eqs. A.44 and A.51), θ_N to the intracellular Chl:N ratio, and nphy and nchl are equal to 0.06 in the model for both PHYS and PHYL. In Eqs. 10, f_{nr}^{PP} refers to the nutrient-replete carbon specific primary production rate (see Eq. A.4), and $h_{Q_{\text{C}}}^{\text{PHY}}$ is given by Eq. 2. The remaining parameters involved in Eqs. 10 are defined in Tab. 6.

2.3 Parameters

The parametrization of such large models is a real challenge. From version to version, some parameters have evolved since the original version of Alekseenko et al. (2014), in order to build up a more and more consistent set of parameters. The underlying idea is to build a parameter set in which most of the parameters would be derived from a subset of reference parameters. Maximum mean cell sizes, maximum specific growth rates $\bar{\mu}$ as well as minimum cell quotas in each PFT, belong to this subset of parameters. For example, maximum intracellular quotas as well as minimum and maximum intracellular ratios have been derived from minimum cell quotas, as done in Thingstad (2005). In the same way, maximum uptake rates have been derived from $\bar{\mu}$ and maximum intracellular quotas, and the associated half-saturation constants from mean cell sizes, based on mechanistic considerations relating the uptake rate of a given nutrient to the external diffusion flux when uptake is limited by external diffusion (Kiorboe, 2008). For grazing, it has also been verified that the parameters used in Eq. A.10, be they taken from the literature or arbitrarily fixed, could supply the predator with sufficient food at steady state when their growth is maximum. If this is not the case, the parameter has been changed accordingly. All parameter values and more details on the relationships between parameters are given in A.3.2.

2.4 The physical model NEMO-MED12

The model results from an off-line coupling between the hydrodynamic NEMO (Nucleus for European Modelling of the Ocean) model (team Madec and NEMO, 2016) and the biogeochemical model Eco3M-MED. The NEMO-MED12 configuration, with a horizontal grid with a resolution of $1/12^\circ$, i.e. grid cells of 6.5 to 8 km, and a vertical resolution of 75 levels with a thickness varying from 1 m on the surface to 135 m on the bottom has been used. It covers the entire Mediterranean Sea and includes a buffer zone from the Strait of Gibraltar to 11 degrees west where the open boundary conditions are gradually applied to avoid numerical instability. The physical simulation used here is called “NM12-FREE” (Hamon et al., 2016) and was run without re-analysis or data assimilation. It covers the period 1979 to June 2013. The initial conditions of the physical variables are taken from monthly averages from the World Ocean Atlas (WOA) and MEDATLAS databases. The freshwater river inputs are taken from the inter-annual data of Ludwig et al. (2009). The Black Sea is not included in this configuration but the freshwater flow of the strait is taken into account. The atmospheric forcing is based on a re-interpolation of the ERA-Interim reanalysis (Dee et al., 2011) with a horizontal resolution of 12 km. The “MN12-FREE” simulation is described in detail in Hamon et al. (2016).

2.5 Satellite data

Ocean colour satellite data are used for the assessment of model outputs. Here, we used a daily surface chlorophyll product supplied by the Copernicus Marine Environment Monitoring Service (CMEMS). In this product, chlorophyll concentrations have been derived using the MEDOC4 algorithm developed by Volpe et al. (2007). This algorithm was built using a large data set of chlorophyll concentrations collected in situ and reflectance measurements from three satellites (SeaWiFS, MERIS and MODIS), constituting a homogeneous set from September 1997.

2.6 Implementation and resolution

The numerical resolution of the transport equation is performed here by the circulation ocean model NEMO-MED12. The 37 state variables of the Eco3M-Med model are then advected and diffused by the physical model. The (sources less sinks) term, hereafter SMS term involved in the transport equation for each state variable is calculated by the biogeochemical model. The resolution is explicit in time, and hence, every 20 min, Eco3M-Med provides the 37 SMS terms to the physical model in each mesh grid cell. SMS terms are calculated for each state variable according to the equations provided in A. The ratios and quotas needed for the calculation of each SMS term are derived from the state variables. For example, Q_N^{PHYS} is given by $\frac{\text{PHYS}_N}{\text{PHYS}}$. Finally, each of the 37 state variables are initialized so as to ensure that the different cell elemental quotas and ratios lie in the authorized respective ranges $[Q_X^{\text{min}}; Q_X^{\text{max}}]$ and $[Q_{XY}^{\text{min}}; Q_{XY}^{\text{max}}]$.

3 Results

An extensive comparison of model outputs with data was undertaken. Next, the results focus on cell quotas and some of the specific knowledge they provide.

3.1 Results relative to model skill assessment

First, modelled and measured vertical profiles of NO₃ and PO₄ in the NW Mediterranean (DyFaMed station) are reported in Fig. 3 at different months. For both model outputs and data, a typical seasonal pattern can be seen, with high nutrients values in winter near the sea surface, followed by the exhaustion of nutrients from the sea surface from late spring (i.e. after the spring bloom) to summer. Afterwards, winter mixing brings back nutrients to the sea surface, making them available for the next spring bloom.

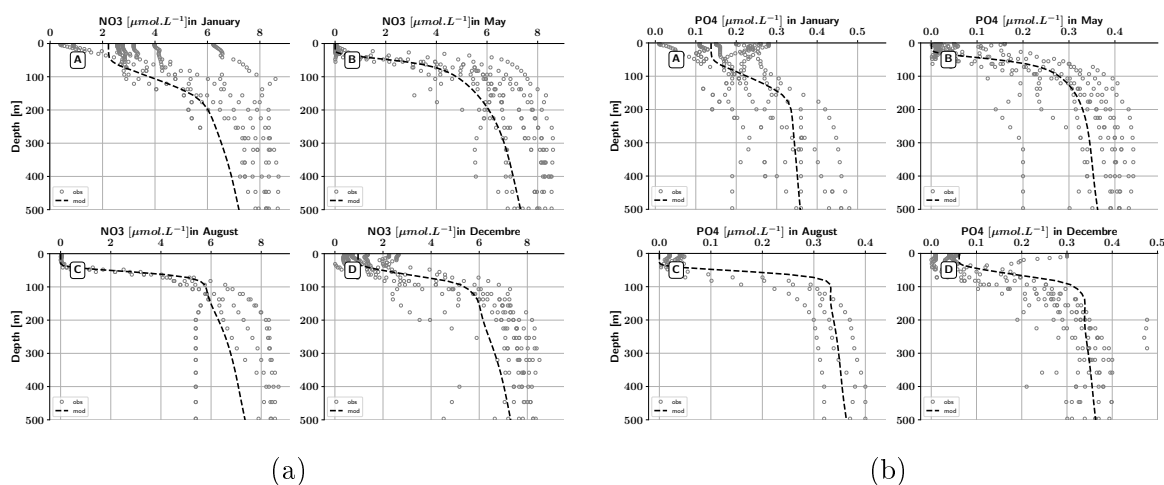


Figure 3: Measured over the 1991-2001 period (circles) and mean over the 1991-2001 period of the modelled (dashed line) nutrients profiles at DyFaMed station in the NW Mediterranean at different seasons. (a) Nitrate (b) Phosphate. In situ data are described in Marty et al. (2002).

Data for the eastern basin are more scarce. Modelled NO₃ and PO₄ profiles are then compared to the few available profiles measured in the Levantine basin during different cruises (Fig. 4). In this case, the seasonality cannot be addressed since these cruises all took place in late spring or summer during which nutrients are exhausted in the surface layer, as shown by both data and model outputs. It can also be noticed that the top nutriclines are deeper in the Levantine basin (4) than in the NW Med (Fig. 3).

A quantitative comparison between satellite Chl data and modelled surface Chl is conducted through a Taylor diagram (Figure 5). The relative RMS error, as well as the correlation and the relative standard deviation between data and model outputs are reported for different sub-basins and for the whole MS. The correlation varies between 0.65 in the Aegean sub-basin and

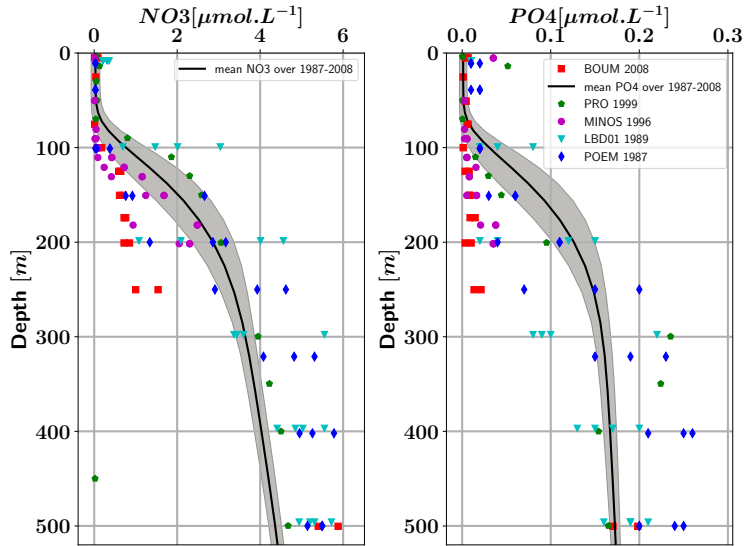


Figure 4: Modelled (full line) and measured (symbols) nutrient profiles measured in the eastern basin during several cruises, namely: POEM 05 (June 1987) in blue; LBD01 (April 1989) in cyan; MINOS (June 1996) in pink; PROSOPE (September 1999) in green and BOUM (July 2008) in red. The modelled nutrient profiles are mean profiles averaged over a region in the Levantin basin encompassing all the stations of the different cruises, and temporally averaged for the period 1987–2008. The grey region represents the temporal standard deviation over the period.

0.97 in the NW and the Adriatic sub-basins. The relative RMS error may be potentially high (up to 0.75), especially in the eastern basin. In the western basin, the error is lower (generally between 0.2 and 0.4), except in the Alboran sub-basin where it is higher (> 0.6). Finally, at MS scale, the relative error is less than 0.6, and the relative standard deviation is roughly within the range 0.6 to 1.3 for all the studied regions, and around 0.7 for the whole MS.

The last comparison concerns cell abundances (Figure 6). The abundance of small phytoplankton is compared with *Synechococcus* and *Prochlorococcus* measured by cytometry, showing an abundance first increasing with depth down to the Deep Chlorophyll Maximum and then decreasing with depth.

3.2 Results relative to cell quotas

The normalized (or relative) surface intracellular C:N ratio of small phytoplankton is quite homogeneous over the basin, roughly varying between 0 and 0.3, except near the south-eastern coast of Tunisia and in the Ionian Sea where C:N values are higher (Fig. 7). Some mesoscale structures with slightly different values of \tilde{Q}_{CN} from the surroundings can however be identified, for example off the Algerian coasts where the mesoscale activity is very intense. By contrast, a

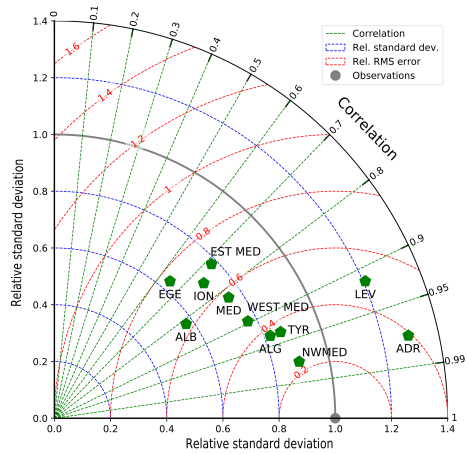


Figure 5: Taylor diagram comparing the modelled and the measured surface chlorophyll over the 1998–2012 period, excluding coastal regions (< 200 m). Observations are provided by the Copernicus Marine Environment Monitoring Service (CMEMS). ALB = Alboran; EGE = Aegean; ION = Ionian; TYR = Tyrrhenian; ALG = Algerian; LEV = Levantine; ADR = Adriatic; EST MED = Eastern Mediterranean Sea; WEST MED = Western Mediterranean Sea; NWMED = North-Western Mediterranean Sea; MED = Mediterranean Sea.

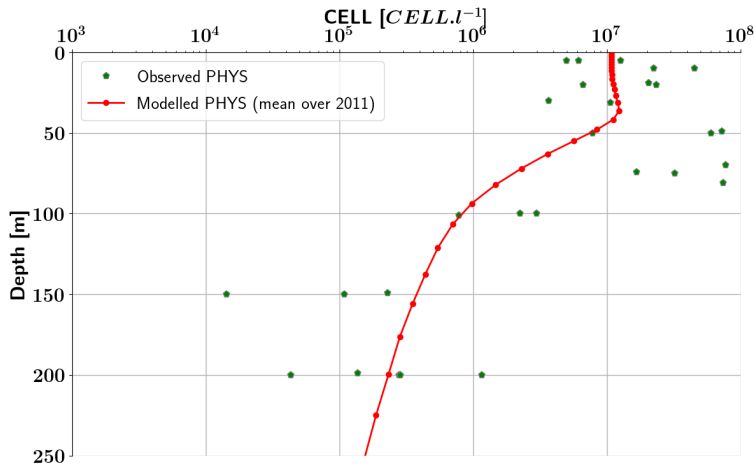


Figure 6: Abundance measurements (green circles) determined by flow cytometry and performed at the PRE-CYM flow cytometry platform of the MIO using a FACSCalibur (BD Biosciences). Measurements have been performed in the NW Mediterranean Sea at the EMSO ANTARES station in 2011. Only the *Synechococcus* and *Prochlorococcus* measured abundances have been plotted. The modelled PHYS (red line) in the same region averaged over year 2011 has been superimposed.

clear west-east gradient of normalized carbon cell quota \tilde{Q}_C can be identified, with \tilde{Q}_C values reaching nearly 0.7 in the Levantine sub-basin. The distribution of the normalized nitrogen cell quota \tilde{Q}_N is more heterogeneous, though with overall PHYS cells that are richer in N in the eastern basin than in the western basin, except in the Ionian sub-basin. It is worth noting that

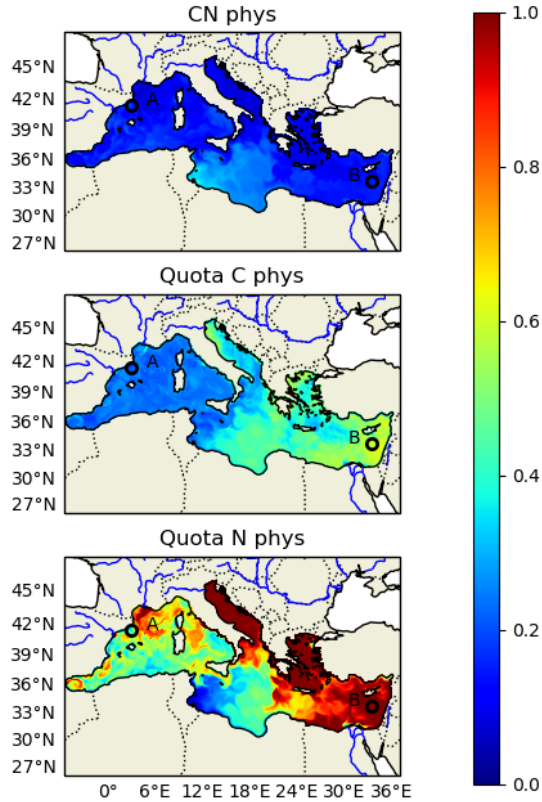


Figure 7: *Normalized intracellular characteristics of small phytoplankton at the sea surface in April 2008 (top) normalized C:N ratio \tilde{Q}_{CN} , (middle) normalized carbon cell quota \tilde{Q}_C , (bottom) normalized nitrogen cell quota \tilde{Q}_N .*

the same value for the C:N ratio can be found in very different regions, such as for example in the NW Med Sea and the Levantine sub-basin: a \tilde{Q}_{CN} value of 0.18 and 0.15 can be found respectively at points A and B (cf Fig. 7), while these two sites correspond to two very different environments and nutritional states for PHYS: at the former (point A), PHYS carbon relative quota is low (0.18), against 0.59 at point B. Moreover, the nitrogen quota is quite moderate at point A (0.34) while cells are N-repleted at point B ($\tilde{Q}_N = 0.99$).

The biogenic element among C, N or P which limits bacterial growth varies with time and space (Fig. 8). If we look at surface waters during winter, heterotrophic bacteria are C-limited in the Western Basin except along the northern coasts and almost everywhere P-limited in the Eastern Basin (except in some particular hydrodynamical structures such as permanent eddies). In the rest of the year, there is a progressive shift from C-limitation to P-limitation everywhere, except in the Alboran Sea and along the Algerian and Tunisian coasts where C-limitation gives way to N-limitation instead (Figure 8(a)). Looking now at the mean limitation over the 0–100 m

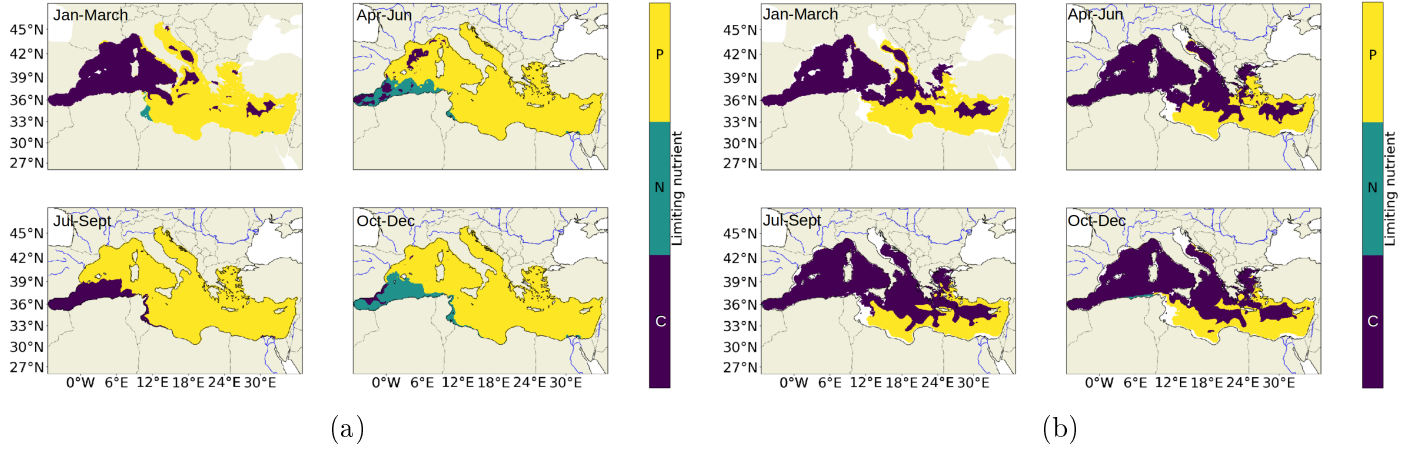


Figure 8: *Biogenic element (among C, N and P) limiting bacterial growth during the four seasons (a) in the surface layer and (b) in the 0–100 m depth layer. The areas coloured in purple are C-limited, the green areas are N-limited and the yellow areas are P-limited.*

layer, things are quite different since growth limitation by carbon expands over the most part of the Mediterranean, the remaining being P-limited, except in the south of the Ionian Sea and in some regions of the Levantin Basin which remain P-limited all over the year.

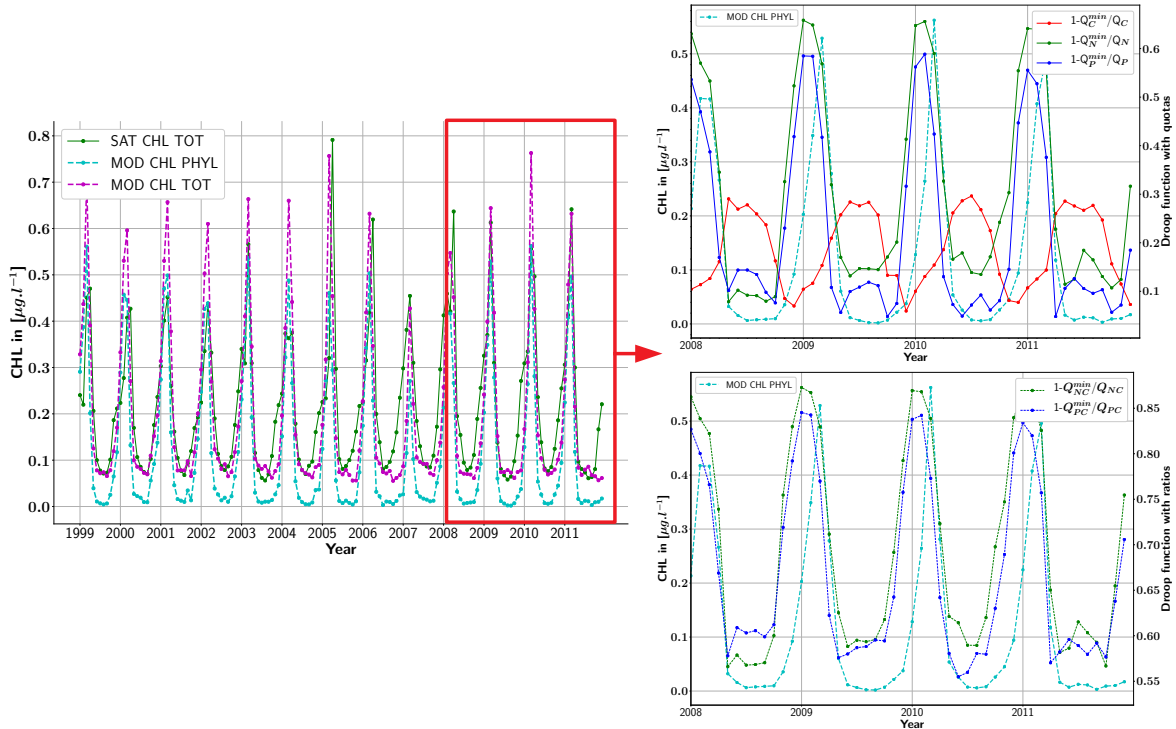


Figure 9: *(left) Temporal evolution over the 1999–2012 period of the modelled and the measured surface Chl in the NW Mediterranean Sea, (right) zoom over the 2008–2012 period of the Droop quota function as given by Eq. A.2 and calculated with (top) the C, N, P quotas of large phytoplankton and (bottom) the C:N and C:P ratios of large phytoplankton. The modelled $PHYL_{CHL}$ is also superimposed on these figures.*

Satellite surface Chl averaged over the NW MED is plotted for the 1999–2012 period as well as the mean total surface Chl calculated by the model (9). The mean surface chlorophyll associated with PHYL is also superimposed on the same figure. The three curves show an alternation between periods of low chlorophyll concentrations ($< 0.1 \mu\text{g l}^{-1}$), roughly between June and November, and periods, between December and May, during which Chl increases rapidly up to a maximum located between 0.45 and $0.8 \mu\text{g l}^{-1}$ depending on the year, before decreasing rapidly below $0.1 \mu\text{g l}^{-1}$. This comparison shows a very strong (qualitative) correlation between the occurrence of the Chl maxima provided by the three curves. In some years (especially from 2004), the bloom takes place in two stages, as evidenced by satellite chlorophyll data. In such situations, a fall bloom of low intensity occurs until a slowdown in Chl production, followed by the onset of the “main bloom” (namely the spring bloom). The model clearly fails to reproduce this fall bloom. Importantly, it can be noticed that PHYL Chlorophyll peaks are well correlated with the spring bloom peaks exhibited by satellite data.

To investigate the link between the occurrence of the spring bloom in the NW Med and the intracellular content of phytoplankton, the modelled PHYL chlorophyll is superimposed on the Droop quota function for growth f_X^{Droop} (see Eq. A.2), either calculated with PHYL C, N, P cell quotas or with C:N and C:P ratios of PHYL (right panels of Fig. 9). For better clarity, only a few years are presented. It can first be seen that the dynamics of the quota functions calculated with Q_{CN} , Q_{CP} , Q_N and Q_P are very similar. Their shape is also similar to that of the modelled PHYL_{CHL} , except that their peaks are wider and earlier. The dynamics of the quota function calculated with Q_C is more sinusoid-like than the other curves and in phase opposition with the latter, with maximum values in summer and minimum values in winter.

The modelled mean vertical nutrients profiles presented in Fig. 10 are the same as those presented in 3 but the normalized intracellular ratios and quotas of bacteria have been superimposed. Since the configurations are quite similar for both NO_3 and PO_4 , only a common description is given. At first glance, it can be seen that the seasonal vertical profiles of the X:C intracellular ratio (\tilde{Q}_{CX}) and that of the carbon quota \tilde{Q}_C are quite similar, and both are roughly symmetrical with the nutrient vertical profiles. In other words, high \tilde{Q}_C and \tilde{Q}_{CX} values coincide with low nutrient values and vice versa and the transition from one situation to the other occurs in the region of the nutriclines. Note that \tilde{Q}_C and \tilde{Q}_{CX} values can significantly differ, mostly in the surface layer, as for example in fall where \tilde{Q}_C values are still very high (around 0.8) while \tilde{Q}_{CX} values are low (around 0.3).

4 Discussion

4.1 Cell quotas as a tool to build a mechanistic and consistent model

Cell quotas and intracellular ratios provide a frame naturally adapted to the mechanistic formulation of biogeochemical processes. Since the pioneering work of several authors (e.g. Droop,

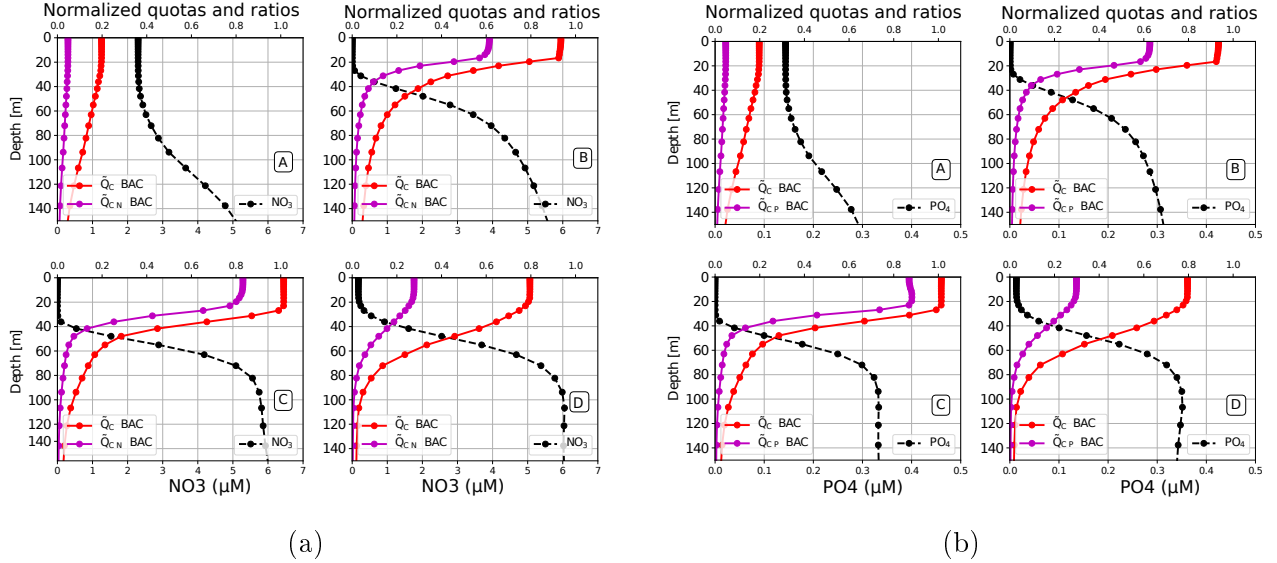


Figure 10: (a) Mean modelled nitrate vertical profile over the 1991–2001 period at the DyfaMed station in (A) January, (B) April, (C) August (D) December. Mean normalized C cell quota and N:C ratios in bacteria are superimposed. (b) Mean modelled phosphate vertical profile over the 1991–2001 period at the DyfaMed station in (A) January, (B) April, (C) August (D) December. Mean normalized C cell quota and P:C ratios in bacteria are superimposed.

1968; Lehman et al., 1975; Geider et al., 1998), there has been a broad consensus on the role of intracellular content in the kinetics of processes undertaken by marine plankton, such as growth, uptake, etc. In practice, cell quotas and intracellular ratios are embedded in quota functions regulating the rate of these processes, as first done by Droop (1968) for phytoplankton growth rate. Since then, several authors (Kooijman, 2000; Lemesle and Mailleret, 2008; Pahlow and Oschlies, 2013) have evidenced the mechanistic foundations of this model. In the same way, several studies have evidenced a relationship between ammonium and phosphate regeneration by bacteria and the C:N ratio of the substrate (Goldman et al., 1987) or the C:N:P ratio of bacteria (Tezuka, 1990), leading bacteria to regenerate ammonium (phosphate) when their C:N(C:P) ratio is low.

However, a given X:Y ratio may correspond to a range of cell quotas Q_X , Q_Y , and therefore to highly contrasted nutritional status of cells (see section 4.3 for more details on this point). This led us to extend the aforementioned knowledge on intracellular ratios to cell quotas, on the underlying assumption that absolute contents of biogenic elements in a cell (and especially that of the most limiting element), rather than – or in addition to – intracellular ratios, may control the rate of biogeochemical processes. For most processes embedded in the model, intracellular ratios still play a role in the regulation of rate, but a “secondary role” (see section 2.2). For a few of them however, namely growth (i.e. cell division rate) and mineralization by bacteria, cell quotas are the only regulators, as done in several other models for the former process (Burmester, 1979; Thingstad, 2005). If heterotrophic bacteria can acquire N and P through

inorganic nutrients, mineralization is their only way to meet their carbon requirements. As such, intracellular carbon and therefore the carbon cell quota in bacteria can be considered to play a particular role in the regulation of the mineralization process. Moreover, there is a consensus in the available experimental results (e.g Goldman et al., 1987; Tezuka, 1990) that NH_4 and PO_4 regeneration by bacteria increases with the decrease of C:N and C:P ratios. Such results are not in contradiction with the fact that the mineralization rate could rather be a function of the Q_C quota in bacteria rather than C:N and C:P since only intracellular ratios are measured. More important is the observation made by these authors that the regeneration of NH_4 and PO_4 by growing bacteria only occurs when the C:N and the C:P ratios of the substrate are below a certain threshold, typically 10:1 and 60:1 respectively for C:N and C:P. This suggests that when bacteria are carbon-repleted (i.e. when their $Q_C = Q_C^{max}$), whatever their intracellular C:N ratio or C:P ratios, the mineralization rate is zero, as is the case in our model.

Moreover, several conclusions can be drawn from Fig. 10 in which quotas and ratios are superimposed on nutrient vertical profiles. First, it can be seen for each biogenic element X , that C:X ratios and the Q_C quota act in the same direction, and that, as a first approximation, a regulation exerted by Q_C on the mineralization of element X is not inconsistent with a regulation by C:X ratio. However, the surface value of Q_C can significantly differ from that in C:X, especially in late summer and winter. This suggests that if the mineralization rate was controlled by C:X instead of Q_C , it would be much higher, leading to an overestimation of nutrient concentrations by the model. Also, the shape, and mostly the value, of the quota and ratio curves at a given depth differ. Since these curves will strongly constrain not only the position of the top of the nutriclines, but also the slope of the nutricline, a regulation by C:X ratios would have resulted in nutriclines with different positions and slopes. However, the quite successful representation of the nutriclines' position (Figs. 3 and 4), as well as the model's ability to reproduce and potentially explain the vertical shift between the nitracline and the phosphacline observed in situ in the eastern MS (Pagès et al., 2020b), suggest that the bacterial carbon cell quota could indeed be the factor actually regulating the mineralization process by heterotrophic bacteria (though dedicated experiments would be the best way to confirm this assumption).

Cell quotas are also useful to establish coherent relationships between parameters. The model consistency is indeed improved when using a consistent set of parameters rather than a set of parameters made up of values gathered in literature and associated with different in situ or laboratory experiments and conditions. It is for example known that under steady-state conditions, the cell quota is the quotient of the specific rates of uptake and growth (Droop, 1968), and the maximum uptake rate can therefore be derived from the maximum growth rate (see Eq. A.22) using the maximum cell quota. In the same way, cell quotas can also be used to derive maximum food supply needs for zooplankton, and therefore to obtain parameters such as the maximum ingestion rate (see Tab. 3 and 4).

The introduction of PFT abundances as state variables into the model, required to derive cell quotas, provides additional data to be compared with in situ measurements (see section 3.1). Furthermore, using abundances in addition to biomasses makes it possible to distinguish phytoplankton growth from photosynthesis and uptake. It is indeed only under conditions of steady-state – a condition rarely achieved in natural environments – that the uptake rate of nutrients is equivalent to growth or the rate of photosynthesis equal to growth (Glibert et al., 2013, and references herein). In the same way, bacterial production and bacteria cell division rate can also be distinguished when using bacteria abundance.

4.2 Benefits of cell quotas with regard to model skill

With the increasing number of studies using coupled biogeochemical/physical models in oceanography, the question of model validation has arisen, especially for the biogeochemical compartment in which the complexity of biological processes in the ocean presents enormous difficulties beyond physics (Lynch et al., 2009). Several studies (e.g. Arhonditsis and Brett, 2004; Stow et al., 2009) have addressed this question, highlighting the relatively low skill assessment rate of such models in literature, and pointing out the need for dedicated quantitative metrics. Some of these metrics have been used in the Results section, and in other papers (Pagès et al., 2020b). However, the use of a root mean squared error (RMSE) or an average error to measure the size of the discrepancies between predicted and observed values can be excessively unfavourable in some cases. For example, the point-by-point comparison of modelled chlorophyll with a satellite-derived surface chlorophyll map using a RMSE may indicate a poor performance of the model while the model produces a good representation of the main features albeit with a slight spatial shift.

The difficulty of quantifying model skill also lies in the scarcity of data, though several technologies (gliders, drifting floats, etc.) have considerably increased the amount available in the last decade, at least for some variables (namely chlorophyll a and macro-nutrients). However, biogeochemical models generally encompass many more state variables than chlorophyll and nutrients, for which no data, or a very limited amount, are available. In this context, cell abundances as used in the present model provide an additional opportunity for comparison with data, with the double benefit that they are direct data (useable without any conversion factor), and that they can be available at high time frequency with the recent technology of automated and autonomous Cytobuoy b.v. flow cytometers for in situ operation (Dubelaar et al., 1999; Thyssen et al., 2008; Marrec et al., 2018; Rousselet et al., 2019).

4.3 Cell quotas allow a deeper comprehension of trophic relations and ecosystem functioning

Cell quotas differ from intracellular ratios in that they are absolute quantities while intracellular ratios are relative quantities. As such, the information provided by intracellular ratios is only

partial. This is well illustrated by Fig. 7 in which a given C:N ratio value may correspond to very contrasted nutritional state of cells in terms of carbon and nitrogen. Hence, the information provided by intracellular ratios is only partial and cannot be used alone for a full characterization of the nutrient status of organisms in the planktonic food web, or an in-depth analysis and comprehension of the associated biogeochemical fluxes.

Another possibility offered by models including cell quotas and abundances is that both the cellular/individual and the population scales can be captured. As an example, the time delay between a phosphate enrichment in phosphate-limited waters in a mesocosm and the increase in primary production that was observed several days later, could be explained and reproduced using a model very similar to the present one except that diazotrophs have been included. In substance, the model revealed that at individual scale, the effect of the phosphate enrichment was immediate (the P quota increased rapidly in planktonic cells after the enrichment) while it took more than five days before the effect at population scale, namely the increase in PP, could be observed (Gimenez et al., 2016). This study also suggested that classical short-term (i.e. around two-day long) microcosm experiments used to quantify nutrient limitations of primary production should be called into question.

The suitability of cell quotas to be used as a proxy for nutritional quality is another important feature. The nutritional quality of organisms present in the ecosystem indeed affects not only their own growth potential, but also the activities of other organisms. This is well illustrated by prey-predator interactions where the nutritional value of the prey is a key aspect of the predator population success (Glibert et al., 2013). In this respect, using another very similar model to the present one, except that it includes the ctenophore *Mnemiopsis leidyi* (ML), it has been shown that for a given available prey biomass, ML population abundance was maximum for the prey with the highest nutritional value (Alekseenko et al., 2019). In other words, when considering a given number of prey of low quality versus a lower number of prey with higher nutritional quality, the carbon biomass of prey being identical in the two situations, the population growth of the predator is higher in the latter situation. This stoichiometric modulation of predation (SMP) as defined by Mitra and Flynn (2005) is made possible by the representation of each PFT in terms of an abundance in addition to one or several biomasses, thereby allowing the use of functional responses for grazing expressed in terms of individuals of prey per individuals of predators. Hence, as mentioned by Glibert et al. (2013), "robust foodweb/ecosystem models should incorporate not only kinetic parametrization, but also sufficient description of material composition that relates to nutrition". The introduction of cell quotas in biogeochemical models is therefore a significant contribution towards this end.

Furthermore, for metazoans, intracellular quotas can also be seen as a proxy of size. In Pagès et al. (2020b), using the same model as the one presented in this study (see A), a reduction of the carbon quota in copepods has been simulated by the model over the period 1985–2010, due to the reduction in phosphate inputs from the Mediterranean rivers. Considering that this reduction in carbon quota can be interpreted as a reduction in copepod size, this result could

provide a possible explanation for the reduction in size of small pelagic fishes observed over the last decades (Voulgaridou and Stergiou, 2003; Saraux et al., 2019) since they mainly feed on copepods. Cell quotas were also helpful to fully explain the mechanisms of DOC accumulation in MS surface water during summer (Guyennon et al., 2015).

In the present study, other benefits of cell quotas are highlighted. First, as already mentioned, they complete the information provided by intracellular ratios alone since a given intracellular ratio may correspond to very different nutritional states of organisms (see Figure 2). Moreover, which of the biogeochemical elements most limits PFT growth is an important item of information which is easily provided by intracellular ratios, at least when two elements are compared. This is less straightforward when the comparison between three or more elements has to be undertaken. By contrast, the most-limiting element among any number of elements can easily be derived using intracellular quotas. This allowed to verify that the model was able to reproduce the well-known west-east increase of phytoplankton growth limitation by P (e.g. Krom et al., 1991), since N limitation or N/P colimitation of phytoplankton growth were prevailing in the Western Basin and P-limitation was prevailing in the Eastern Basin (see Pagès et al. (2020a), Fig. 7 A and C). For heterotrophic bacteria, the model can reproduce the main results obtained by Van Wambeke et al. (2002) showing that during summer, bacteria in surface waters are P-limited everywhere in the Mediterranean Sea, except in the Alboran Sea, and that a switch from P-limitation towards C-limitation with depth was observed at two contrasted stations respectively in the Northwestern and Southeastern (Ionian) Mediterranean Sea. The outputs of our model are in agreement with these observations since C-limitation is observed in the Alboran Sea all along the year, and especially during summer (i.e. the period of the above mentioned study), while P-limitation is observed everywhere else during that season (Fig. 8(a)). The switch from P to C limitation of bacterial production (BP) with depth at the two aforementioned contrasted stations is also reproduced by the model since the most limiting element switch to carbon when the analysis is done on the 0–100 m layer (see Fig. 8(b)). Intracellular quotas also allow to evidence some seasonal shifts in BP limitation, but only in the surface waters of the Western Mediterranean Sea, namely from C (in winter) to P-limitation everywhere except in the Alboran Sea and along the Algerian and Tunisian coasts where the shift is from C to N-limitation according to the model (Fig. 8(a)) and these results are consistent with the enrichment experiments performed in the NW Mediterranean by Pinhassi et al. (2006). Switches from C-limitation (in winter, especially in the Western Basin) to N and/or P limitation also occur according to the model for both the small and large phytoplankton (results not shown). Finally, the most limiting nutrient (here denoted X_l) can itself be present at different levels in the $[Q_{X_l}^{\min}; Q_{X_l}^{\max}]$ range associated with this element. This information is of fundamental importance since, according to the value of Q_{X_l} , cell division and population growth can occur or not. As an example, regarding the C:N ratio of small phytoplankton in April (Fig. 7), it is quite homogeneous over the Mediterranean Sea, except perhaps in the

region of the Gulf of Gabes and the Ionian Sea, thus suggesting that PHYS cells are roughly in the same nutritional state throughout the MS. However, when looking at the carbon and nitrogen quotas for PHYS, the conclusion is not really the same, rather suggesting that, at basin scale, PHYS cells are more and more rich in carbon when going eastward. The analysis of nitrogen quotas is less straightforward, exhibiting the highest values where PHYS is either strongly P-limited as in the Levantine basin (results not shown) or located in a nitrogen-rich region (Adriatic Sea, region of the bloom in the NW MS, etc.). In short, access to information provided by cell quotas allows a more in-depth analysis of the effective nutritional state of organisms and thereby of the associated biogeochemical processes and fluxes.

Another interesting item of information provided by intracellular quotas concerns the occurrence of the spring bloom. The purpose here is not to propose a new theory to explain the onset of the bloom on the basis of a combination of physical (e.g. mixed layer depth) and biological (e.g. phytoplankton grazing by zooplankton) considerations. A very large body of literature has already been dedicated to this purpose, from Sverdrup’s precursor critical depth theory (Sverdrup, 1953) that the vernal, or spring, bloom is initiated when the mixed layer depth becomes shallower than the critical depth. Taking into account its underlying hypothesis, and some unsuccessful comparisons with in situ data and with other theoretical models, this theory has been widely debated in the literature (e.g. Huisman et al., 1999; Irigoien et al., 2005; Behrenfeld, 2010) and a synthesis of the different theories established since Sverdrup’s work has for example been proposed in Lindemann and St. John (2014) for the North-Atlantic. Here, we rather aim to focus on the link between the intracellular status of phytoplankton, and especially large phytoplankton (PHYL), and the occurrence of the spring bloom. As already mentioned, though the model fails in representing the fall bloom, there is a strong (qualitative) correlation between the spring bloom exhibited by satellite data and the modelled PHYL chlorophyll (see Fig. 9). The modelled PHYL_{CHL} can therefore be used to explore the link between the spring bloom and the nutritional status of PHYL. The first conclusion that can be drawn is that the C:N and C:P ratios alone are insufficient to fully explain the spring bloom dynamics. If in fall, the increase in PHYL_{CHL} and that in both quota functions calculated with ratios are simultaneous, suggesting that the recovery of nutrients through vertical mixing is the first starter of the increase in PHYL_{CHL}, nothing can be derived from these ratios either concerning the moment of the occurrence of the bloom peak (the peaks of the ratio curves and PHYL_{CHL} curve are staggered), or its intensity since the dynamics of PHYL_{CHL} and quota function curves differ. The information lacking can be provided by the quota functions involving cell quotas which allow the following steps to be identified (note that in order to alleviate the text, the X quota Q_X will sometimes be used instead of the quota function based on Q_X (i.e. f_X^{Droop}) since both develop in the same direction, either increasing or decreasing): As early as October and no later than November, a rapid and simultaneous increase in f_N^{Droop} and f_P^{Droop} occurs, indicating as already suggested with ratios, that growth was nutrient-limited so far, and more

precisely P-limited. This increase is accompanied by an increase in PHYL_{CHL} , but the latter is far less rapid. Two explanations can be put forward to explain this difference. First, quotas are representative of the nutritional status at the cell scale, while PHYL_{CHL} is an indicator at the population scale, and there is a time-lag of a few days between the response at cell scale and at population scale that has already been evidenced and discussed in Gimenez et al. (2016). The second explanation lies in the dynamics of Q_C and thereby that of f_C^{Droop} : it decreases with solar irradiance from July to December and becomes lower than f_P^{Droop} from November and no later than December. In such conditions, PHYL population growth cannot experience the same (though delayed) rapid increase as that observed in f_P^{Droop} and f_N^{Droop} since it is restrained by the control exerted by Q_C . This control will persist until March, namely the moment of the maximum in PHYL_{CHL} , thereby suggesting that the bloom’s intensity is controlled by Q_C . From April, the nutrient quota functions f_N^{Droop} and f_P^{Droop} , which started to decline from January-February, become weaker than f_C^{Droop} and regain control of population growth and primary production. This situation characterized by low Q_N and Q_P values will last until the next autumn when a new cycle will start. In short, the maximum of the bloom peak will occur, almost to the day, at the moment at which Q_C reaches its highest value before the regaining of control by Q_P , with the understanding that external conditions, and especially vertical mixing, will constrain the dynamics of Q_N and Q_P .

5 Conclusion

Biogeochemical models, among which PFT models, have been subject to a number of developments over the last decades. Among them, the introduction of flexible-stoichiometry and the associated intracellular ratios, has resulted in an enhanced knowledge of the ocean’s biogeochemical dynamics. In this paper, our aim was to go further in this approach, with the introduction, for the description of each PFT, of abundance and the associated intracellular quotas. This has already been done in a few other models before the Eco3M-MED model presented here. To our knowledge, it is however the first model in this category to be used in 3D modelling studies, and the aim of this paper is to highlight the benefits provided by cell quotas. A preliminary work was dedicated to the comparison of model outputs with available data, allowing us to conclude, based on these comparisons and several others presented elsewhere, that the coupled model could be used to study the biogeochemical dynamics of the Mediterranean Sea. This paper also presents the way quotas are used to regulate the kinetics of some of the biogeochemical processes involved in the model, using original formulations such as, for example, for the mineralization process. Based on previous experimental work and on the fact that the position and the slopes of the nutriclines are quite well represented by the model, we suggest that mineralization and hydrolysis could indeed be primarily driven by the carbon quota of bacteria, as this is implemented in the model. This paper also aggregates the major results from previous studies based on previous but quite similar versions of the present

model and associated with intracellular quotas. The model could indeed highlight the time-lag between the short-term response of organisms at individual scale (the effect of a phosphate enrichment was immediately perceptible on the P quota of organisms) and the more long-term response (several days) at population scale, thereby suggesting that microcosm experiments used to quantify nutrient limitations of primary production should not be too short. In the context of another study, it has been shown that for a given available prey biomass, predator population abundance was maximum for the prey with the richest nutritional value, i.e. with the highest intracellular quota. Finally, other interesting aspects have been evidenced in the present paper. It first shows that intracellular quotas provide a more in-depth knowledge on the intracellular status of organisms, since similar intracellular ratios can correspond to very contrasted intracellular quotas and nutritional status, as evidenced here for example in April for small phytoplankton in the Mediterranean Sea. Intracellular quotas were also used to provide a seasonal description of the nutritional status of phytoplankton in the north-western MS in relation with chlorophyll dynamics. Internal conditions for the occurrence and the intensity of the spring bloom have also been explored. These investigations suggests that the carbon quota in phytoplankton could be the main internal driver of the spring bloom since it seems to control phytoplankton growth during winter and until the occurrence of the maximum peak of the bloom, followed by the decrease in chlorophyll coinciding with the moment where N and/or P become more limiting than carbon. Finally, if the introduction of abundances in PFT models increases the computational costs, since the number of state variables and processes is increased, we have attempted to demonstrate throughout this paper that the benefits provided by cell quotas clearly outweigh these costs.

Acknowledgements

This project is part of the Labex OT-Med (no. ANR-11-LABX-0061) funded by the French Government “Investissements d’Avenir” program of the French National Research Agency (ANR) through the A*MIDEX project (no ANR-11-IDEX-0001-02). This work has benefited from HPC resources from GENCI-IDRIS (Grant 2018-0227) and from OSU Pytheas. This study has been conducted using EU Copernicus Marine Service Information. We thank the staff of PRE-CYM for providing the flow cytometry data got in the framework of the MOOSE Project. The National Institute for Earth Science and Astronomy (INSU) of CNRS supports MOOSE with the Alliance ALLENI on behalf of the French research organizations on the environment. We also thank the different experimenter colleagues from MIO for their availability for discussions on biogeochemistry, and especially France van Wambeke and Thierry Moutin.

References

- Alekseenko, E., Baklouti, M., Carlotti, F., 2019. Main factors favoring *mnemiopsis leidyi* individuals growth and population outbreaks : a modelling approach. *Journal of Marine Systems* 196, 14–35.
- Alekseenko, E., Raybaud, V., Espinasse, B., Carlotti, F., Queguiner, B., Thouvenin, B., Garreau, P., Baklouti, M., 2014. Seasonal dynamics and stoichiometry of the planktonic community in the NW Mediterranean Sea; a 3D modeling approach. *Ocean Dynamics* 64, 179–207.
- Arhonditsis, G. B., Brett, M. T., 2004. Evaluation of the current state of mechanistic aquatic biogeochemical modeling. *Marine Ecology Progress Series* 271, 13–26.
- Aumont, O., Maier-Reimer, E., Blain, S., Monfray, P., 2003. An ecosystem model of the global ocean including Fe, Si, P colimitations. *Global Biogeochemical Cycles* 17(2).
- Ayata, S.-D., Lévy, M., Aumont, O., Sciandra, A., Sainte-Marie, J., Tagliabue, A., Bernard, O., 2013. Phytoplankton growth formulation in marine ecosystem models: Should we take into account photo-acclimation and variable stoichiometry in oligotrophic areas? *Journal of Marine Systems* 125, 29 – 40, advances in Marine Ecosystem Modelling Research III.
- Baklouti, M., Diaz, F., Pinazo, C., Faure, V., Queguiner, B., 2006a. Investigation of mechanistic formulations depicting phytoplankton dynamics for models of marine pelagic ecosystems. *Progress in Oceanography* 71(1), 1–33.
- Baklouti, M., Faure, V., Pawlowski, L., Sciandra, A., 2006b. Investigation and sensitivity analysis of a mechanistic phytoplankton model implemented in a new modular numerical tool (Eco3M) dedicated to biogeochemical modelling. *Progress in Oceanography* 71(1), 34–58.
- Baretta, J., Ebenhoh, W., Ruardij, P., 1995. The European Regional Seas Ecosystem Model, a complex marine ecosystem model. *J. Sea Res.* 33, 233–246.
- Behrenfeld, M. J., 2010. Abandoning sverdrup’s critical depth hypothesis on phytoplankton blooms. *Ecology* 91 (4), 977–989.
- Bopp, L., Resplandy, L., Orr, J. C., Doney, S. C., Dunne, J. P., Gehlen, M., Halloran, P., Heinze, C., Ilyina, T., Séférian, R., Tjiputra, J., Vichi, M., 2013. Multiple stressors of ocean ecosystems in the 21st century: projections with CMIP5 models. *Biogeosciences* 10 (10), 6225–6245.
- Burmester, D. E., 1979. The unsteady continuous culture of phosphate-limited *monochrysis lutheri* droop: Experimental and theoretical analysis. *Journal of Experimental Marine Biology and Ecology* 39 (2), 167 – 186.

- Christaki, U., Courties, C., Joux, F., Jeffrey, W. H., Neveux, J., Naudin, J., 2009. Community structure and trophic role of ciliates and heterotrophic nanoflagellates in Rhone River diluted mesoscale structures (NW Mediterranean Sea). *Aquat Microb Ecol* 57, 263–277.
- Christaki, U., Jacquet, S., Dolan, J. R., Vaulot, D., Rassoulzadegan, F., 1999. Growth and grazing on prochlorococcus and synechococcus by two marine ciliates. *Limnol. Oceanogr.* 44(1), 52–61.
- Christian, J. R., 2005. Biogeochemical cycling in the oligotrophic ocean: Redfield and non-redfield models. *Limnology and Oceanography* 50(2), 646–657.
- Dee, D. P., Uppala, S. M., Simmons, A. J., Berrisford, P., Poli, P., Kobayashi, S., Andrae, U., Balmaseda, M. A., Balsamo, G., Bauer, P., Bechtold, P., Beljaars, A. C. M., Berg, L. V. D., Bidlot, J., Bormann, N., Delsol, C., Dragani, R., Fuentes, M., Geer, A. J., 2011. The ERA-Interim reanalysis : configuration and performance of the data assimilation system. *Royal meteorological society* (April), 553–597.
- Droop, M. R., 1968. Vitamin B-12 and marine ecology. 4. the kinetics of uptake, growth and inhibition in *Monochrysis lutheri*. *J. Mar. Biol. Assoc. U.K.* 48, 689–733.
- Dubelaar, G. B., Gerritzen, P. L., E., B. A., Jonker, R. R., Tangen, K., 1999. Design and first results of cytobuoy: a wireless flow cytometer for in situ analysis of marine and fresh waters. *Cytometry* 37(4), 247–254.
- Fasham, M. J. R., Ducklow, H. W., McKelvie, S. M., 1990. A nitrogen-based model of plankton dynamics in the oceanic mixed layer. *Journal of Marine Research* 48, 591–639.
- Flynn, K. J., 2003. Modelling multi-nutrient interactions in phytoplankton; balancing simplicity and realism. *Progress in Oceanography* 56, 249–279.
- Flynn, K. J., 2010. Ecological modelling in a sea of variable stoichiometry: Dysfunctionality and the legacy of Redfield and Monod. *Progress In Oceanography* 84 (1-2), 52 – 65, special Issue: Parameterisation of Trophic Interactions in Ecosystem Modelling.
- Follows, M. J., Dutkiewicz, S., 2011. Modeling diverse communities of marine microbes. *Annual Review of Marine Science* 3, 427–451.
- Franks, P. J. S., 2002. NPZ models of plankton dynamics: Their construction, coupling to physics, and application. *Journal of Oceanography* 58 (2), 379–387.
- Geider, R. J., MacIntyre, H. L., Kana, T. M., 1998. A dynamic regulatory model of phytoplanktonic acclimation to light, nutrients, and temperature. *Limnology and Oceanography* 43(4), 679–694.

- Gimenez, A., Baklouti, M., Bonnet, S., Moutin, T., 2016. Biogeochemical fluxes and fate of diazotroph derived nitrogen in the food web after a phosphate enrichment: Modeling of the vahine mesocosms experiment. *Biogeosciences* 13, 5103–5120.
- Gimenez, A., Baklouti, M., Wagener, T., Moutin, T., 2018. Diazotrophy as the main driver of the oligotrophy gradient in the western tropical south pacific ocean: results from a one-dimensional biogeochemical–physical coupled model. *Biogeosciences* 15 (21), 6573–6589.
- Glibert, P. M., Kana, T. M., Brown, K., 2013. From limitation to excess: the consequences of substrate excess and stoichiometry for phytoplankton physiology, trophodynamics and biogeochemistry, and the implications for modeling. *Journal of Marine Systems* 125, 14 – 28, advances in Marine Ecosystem Modelling Research III.
- Gnanadesikan, A., Dunne, J. P., John, J., 01 2011. What ocean biogeochemical models can tell us about bottom-up control of ecosystem variability. *ICES Journal of Marine Science* 68 (6), 1030–1044.
- Goldman, J. C., Caron, D. A., Dennett, M. R., 1987. Regulation of gross growth efficiency and ammonium regeneration in bacteria by substrate C: N ratio. *Limnology and Oceanography* 32 (6), 1239–1252.
- Guyennon, A., Baklouti, M., Diaz, F., Palmieri, J., Beuvier, J., Lebaupin-Brossier, C., Arsouze, T., Béranger, K., Dutay, J. C., Moutin, T., 2015. New insights into the organic carbon export in the Mediterranean Sea from 3D modeling. *Biogeosciences* 12, 7025–7046, doi:10.5194/bg-12-7025-2015.
- Hamon, M., Beuvier, J., Somot, S., Lellouche, J.-M., Greiner, E., Jordà, G., Bouin, M.-n., Arsouze, T., Sevault, F., 2016. Design and validation of MEDRYS , a Mediterranean Sea reanalysis over the period 1992-2013. *Ocean Science*.
- Han, B. P., 2002. A mechanistic model of algal photoinhibition induced by photodamage to photosystem-II. *Journal of Theoretical Biology* 214, 519–527.
- Harrison, W. G., Harris, L. R., Irwin, B. D., 1996. The kinetics of nitrogen utilization in the oceanic mixed layer: Nitrate and ammonium interactions at nanomolar concentrations. *Limnol. and Oceanogr.* 41(1), 16–32.
- Holling, C., 1959. Some characteristics of simple types of predation and parasitism. *Canadian Entomologist* 91, 385–398.
- Huisman, J., van Oostveen, P., Weissing, F. J., 1999. Critical depth and critical turbulence: Two different mechanisms for the development of phytoplankton blooms. *Limnology and Oceanography* 44 (7), 1781–1787.

- Irigoien, X., Flynn, K. J., Harris, R. P., 2005. Phytoplankton blooms: a "loophole" in microzooplankton grazing impact? *Journal of Plankton Research* 27 (4), 313–321.
- Kiorboe, T., 2008. *A Mechanistic Approach to Plankton Ecology*. Princeton University Press.
- Klausmeier, C., Litchman, E., Daufresne, T., Levin, S., May 2008. Phytoplankton stoichiometry. *Ecological Research* 23 (3), 479–485.
- Klausmeier, C. A., Litchman, E., Levin, S. A., 2004. Phytoplankton growth and stoichiometry under multiple nutrient limitation. *Limnology and Oceanography* 49 (4part2), 1463–1470.
- Kooijman, S. A. L. M., 2000. *Dynamic Energy and Mass Budgets in Biological Systems*. Cambridge University Press, Cambridge, UK.
- Krom, M. D., Kress, N., Brenner, S., 1991. Phosphorus limitation of primary productivity in the eastern mediterranean sea. *Limnol. Oceanogr.* 36 (3), 424–432.
- Lazzari, P., Solidoro, C., Ibello, V., Salon, S., Teruzzi, A., Béranger, K., Colella, S., Crise, A., 2012. Seasonal and inter-annual variability of plankton chlorophyll and primary production in the mediterranean sea: a modelling approach. *Biogeosciences* 9 (1), 217–233.
- Lazzari, P., Solidoro, C., Salon, S., Bolzon, G., 2016. Spatial variability of phosphate and nitrate in the mediterranean sea: A modeling approach. *Deep Sea Research Part I: Oceanographic Research Papers* 108, 39 – 52.
- Lehman, J. T., Botkin, D. B., Likens, G. E., 1975. The assumptions and rationales of a computer model of phytoplankton population dynamics. *Limnol. and Oceanogr.* 20(3), 343–364.
- Lemesle, V., Mailleret, L., 2008. A mechanistic investigation of the algae growth Droop model. *Acta Biotheor.* 56(1-2), 87–102.
- Letscher, R. T., Moore, J. K., Teng, Y.-C., Primeau, F., 2015. Variable c : N : P stoichiometry of dissolved organic matter cycling in the community earth system model. *Biogeosciences* 12 (1), 209–221.
- Lévy, M., Martin, A. P., 2013. The influence of mesoscale and submesoscale heterogeneity on ocean biogeochemical reactions. *Global Biogeochemical Cycles* 27 (4), 1139–1150.
- Lindemann, C., St. John, M. A., 2014. A seasonal diary of phytoplankton in the north atlantic. *Frontiers in Marine Science* 1, 37.
- Ludwig, W., Dumont, E., Meybeck, M., Heussner, S., 2009. River discharges of water and nutrients to the Mediterranean and Black Sea: Major drivers for ecosystem changes during past and future decades? *Progress in Oceanography* 80 (3-4), 199–217.

- Lynch, D. R., Jr., D. J. M., Werner, F. E., 2009. Skill assessment for coupled biological/physical models of marine systems. *Journal of Marine Systems* 76 (1-2), 1 – 3.
- Macias, D., Huertas, I. E., Garcia-Gorriz, E., Stips, A., 2019. Non-redfieldian dynamics driven by phytoplankton phosphate frugality explain nutrient and chlorophyll patterns in model simulations for the Mediterranean Sea. *Progress in Oceanography* 173, 37 – 50.
- Marrec, P., Grégori, G., Doglioli, A. M., Dugenne, M., Della Penna, A., Bhairy, N., Cariou, T., Hélias Nunige, S., Lahbib, S., Rougier, G., Wagener, T., Thyssen, M., 2018. Coupling physics and biogeochemistry thanks to high-resolution observations of the phytoplankton community structure in the northwestern mediterranean sea. *Biogeosciences* 15 (5), 1579–1606.
- Marty, J.-C., Chiavérini, J., Pizay, M.-D., Avril, B., 2002. Seasonal and interannual dynamics of nutrients and phytoplankton pigments in the western mediterranean sea at the dyfamed time-series station (1991–1999). *Deep Sea Research Part II: Topical Studies in Oceanography* 49 (11), 1965–1985, studies at the DYFAMED (France JGOFS) Time-Series Station, N.W. Mediterranean Sea.
- Mauriac, R., Moutin, T., Baklouti, M., 2011. Accumulation of DOC in Low Phosphate Low Chlorophyll (LPLC) area: Is it related to higher production under high N:P ratio ? *Biogeosciences* 8 (4), 933–950.
- Mitra, A., Flynn, K. J., 2005. Predator-prey interactions: is 'ecological stoichiometry' sufficient when good food goes bad? *Journal of Plankton Research* 27 (5), 393–399.
- Pagès, R., Baklouti, M., Barrier, N., Ayache, M., Sevault, F., Somot, S., Moutin, T., 2020a. Projected effects of climate-induced changes in hydrodynamics on the biogeochemistry of the Mediterranean Sea under the RCP 8.5 regional climate scenario. *Frontiers in Marine Science* 7, 957.
- Pagès, R., Baklouti, M., Barrier, N., Richon, C., Dutay, J.-C., Moutin, T., 2020b. Changes in rivers inputs during the last decades significantly impacted the biogeochemistry of the eastern mediterranean basin: A modelling study. *Progress in Oceanography* 181, 102242.
- Pahlow, M., Oschlies, A., 2013. Optimal allocation backs Droop's cell-quota model. *Marine Ecology Progress Series* 473, 1–5.
- Perez, M. T., Dolan, J. R., Fukai, E., 1997. Planktonic ologotrophic ciliates in the NW Mediterranean: growth rates and consumption by copepods. *Marine Ecology Progress Series* 155, 89–101.
- Pinhassi, J., Gómez-Consarnau, L., Alonso-Sáez, L., Sala, M. M., Montserrat Vidal, M. Pedrós-Alió, C., Gasol, J. M., 2006. Seasonal changes in bacterioplankton nutrient limitation and

- their effects on bacterial community composition in the nw mediterranean sea. *AQUATIC MICROBIAL ECOLOGY* 44, 241–252.
- Poggiale, J. C., Baklouti, M., Queguiner, B., Kooijman, B., 2010. How far details are important in ecosystem modelling: the case of multi-limiting nutrients in phytoplankton - zooplankton interactions. *Phil. Trans. R. Soc. B* 365, 3495–3507.
- Riley, G. A., 1946. Factors controlling phytoplankton population on george's bank. *J. Mar. Res.* 6, 54–73.
- Rousselet, L., Doglioli, A. M., de Verneil, A., Pietri, A., Della Penna, A., Berline, L., Marrec, P., Grégori, G., Thyssen, M., Carlotti, F., Barrillon, S., Simon-Bot, F., Bonal, M., d'Ovidio, F., Petrenko, A., 2019. Vertical motions and their effects on a biogeochemical tracer in a cyclonic structure finely observed in the ligurian sea. *Journal of Geophysical Research: Oceans* 124 (6), 3561–3574.
- Salihoglu, B., Garcon, V., Oschlies, A., Lomas, M., 2008. Influence of nutrient utilization and remineralization stoichiometry on phytoplankton species and carbon export: A modeling study at bats. *Deep Sea Research Part I: Oceanographic Research Papers* 55 (1), 73 – 107.
- Saraux, C., Beveren, E. V., Brosset, P., Queiros, Q., Bourdeix, J.-H., Dutto, G., Gasset, E., Jac, C., Bonhommeau, S., Fromentin, J.-M., 2019. Small pelagic fish dynamics: A review of mechanisms in the gulf of lions. *Deep Sea Research Part II: Topical Studies in Oceanography* 159, 52 – 61, drivers of dynamics of small pelagic fish resources: environmental control of long-term changes.
- Sherr, E. B., Rassoulzadegan, F., Sherr, B. F., 1989. Bacterivory by pelagic choreotrichous ciliates in coastal waters of the NW Mediterranean Sea. *Marine Ecology Progress Series* 55, 235–240.
- Smirnov, N. A., Revkova, N. V., Mar 2002. Estimates of cell quotas of nitrogen and phosphorus in accumulative cultures of chlorococcous algae. *Biology Bulletin of the Russian Academy of Sciences* 29 (2), 185–191.
- Steele, J. H., Henderson, E. W., 1981. A simple plankton model. *The American Naturalist* 117 (5), 676–691.
- Stock, C. A., Dunne, J. P., John, J. G., 2014. Global-scale carbon and energy flows through the marine planktonic food web: An analysis with a coupled physical–biological model. *Progress in Oceanography* 120, 1 – 28.
- Stow, C. A., Jolliff, J., McGillicuddy, D. J., Doney, S. C., Allen, J. I., Friedrichs, M. A. M., Rose, K. A., Wallhead, P., 2009. Skill assessment for coupled biological/physical models of marine systems. *Journal of Marine Systems* 76 (1-2), 4 – 15.

- Sverdrup, H. U., 01 1953. On Conditions for the Vernal Blooming of Phytoplankton. *ICES Journal of Marine Science* 18 (3), 287–295.
- Tagliabue, A., Bopp, L., Gehlen, M., 2011. The response of marine carbon and nutrient cycles to ocean acidification: Large uncertainties related to phytoplankton physiological assumptions. *Global Biogeochemical Cycles* 25 (3).
- team Madec, G., NEMO, 2016. NEMO ocean engine (27).
- Tezuka, Y., 1990. Bacterial regeneration of ammonium and phosphate as affected by the carbon:nitrogen:phosphorus ratio of organic substrates. *Microbial Ecology* 19 (3), 227–238.
- Thingstad, T., Lignell, R., 1997. Theoretical models for the control of bacterial growth rate, abundance, diversity and carbon demand. *Aquat Microb Ecol* 13 (1), 19–27.
- Thingstad, T. F., 2005. Simulating the response to phosphate additions in the oligotrophic eastern Mediterranean using an idealized four-member microbial food web model. *Deep-Sea Research II* 52, 3074–3089.
- Thyssen, M., Mathieu, D., Garcia, N., Denis, M., 05 2008. Short-term variation of phytoplankton assemblages in Mediterranean coastal waters recorded with an automated submerged flow cytometer. *Journal of Plankton Research* 30 (9), 1027–1040.
- Vallina, S. M., Ward, B. A., Dutkiewicz, S., Follows, M. J., Jan. 2014. Maximal feeding with active prey-switching: A kill-the-winner functional response and its effect on global diversity and biogeography. *Progress in Oceanography* 120, 93–109.
- Van Wambeke, F., Christaki, U., Giannakourou, A., Moutin, T., Souvemerzoglou, K., 2002. Longitudinal and vertical trends of bacterial limitation by phosphorus and carbon in the mediterranean sea. *Microbial Ecology* 43, 119–133.
- Vichi, M., Masina, S., Navarra, A., 2007a. A generalized model of pelagic biogeochemistry for the global ocean ecosystem. part II: Numerical simulations. *Journal of Marine Systems* 64 (1), 110–134.
- Vichi, M., Pinardi, N., Masina, S., 2007b. A generalized model of pelagic biogeochemistry for the global ocean ecosystem. part I: Theory. *Journal of Marine Systems* 64 (1), 89 – 109.
- Volpe, G., Santoleri, R., Vellucci, V., d’Alcalá, M. R., Marullo, S., D’Ortenzio, F., 2007. The colour of the mediterranean sea: Global versus regional bio-optical algorithms evaluation and implication for satellite chlorophyll estimates. *Remote Sensing of Environment* 107 (4), 625 – 638.
- Voulgaridou, P., Stergiou, K., 2003. Trends in various biological parameters of the european sardine, *sardina pilchardus* (walbaum, 1792), in the eastern mediterranean sea. *Scientia Marina* 67 (S1), 269–280.

Weber, T. S., Deutsch, C., 2010. Ocean nutrient ratios governed by plankton biogeography. Nature 467, 550–554.

A Full description of the Eco3M-MED biogeochemical model

This appendix provides a full description of the updated version of the Eco3M-MED model since its original version in Alekseenko et al. (2014). However, the underlying mechanisms depicted by the following mathematical formulations are not extensively described here and can be found in the previous articles already cited in the text.

A.1 State variables

The state variables of the Eco3M-MED model are given in Tab. 1.

A.2 Mathematical formulations for biogeochemical processes

A.2.1 Growth of unicellular plankton functional types

Each unicellular PFT is described in terms of an abundance, the dynamics of which is driven by cell division (the case of the metazoan mesozooplankton is treated apart). The PFT's population specific growth rate f^μ is controlled by the most limiting biogenic element among C, N and P, through the classical Droop quota function combined with Leibig's law of the minimum:

$$f^\mu = \bar{\mu} \cdot \min_X \left(f_X^{Droop} \right) \quad (\text{A.1})$$

In this formulation, $\bar{\mu}$ stands for the maximum theoretical specific growth rate of the PFT's population, and f_X^{Droop} for the Droop quota function (see Eq. A.2) in which Q_X stands for the intracellular content in a given element X among C, N and P:

$$f_X^{Droop} = \left(1 - \frac{Q_X^{\min}}{Q_X} \right) \quad (\text{A.2})$$

A.2.2 Growth of mesozooplankton

Eq. A.1 is also used to describe the dynamics of mesozooplankton population (Z), i.e. the specific population growth rate (which corresponds to egg production rate). The life phase between egg and adult stages, i.e. the "juvenile phase", is not explicitly represented. Instead, as spawning occurs, the entire amount of material required to grow from egg stage to young adult stage is instantly and explicitly transferred from the prey biomass pools (PHYL, CIL and HNF) to the adult pool (see Eq. A.3). In other words, the time-lag between the egg and adult stages is not accounted for by the model, but the accumulated ingested food needed for the juvenile growth is explicitly taken into account through implicit Z juvenile grazing on Z prey. This grazing during juvenile stages is implicitly represented in the model through the following expression:

$$f_z^{gg^{jvw}} = 0.85 \cdot Q_C^{Z,\min} \cdot f_z^\mu \quad (\text{A.3})$$

Table 1: *List of the model's state variables and associated acronyms and units*

Variables	Notations	Units
Mesozooplankton abundance	Z	ind l ⁻¹
Mesozooplankton carbon concentration	Z _C	(mol C) l ⁻¹
Ciliate cellular abundance	CIL	cell l ⁻¹
Ciliate carbon concentration	CIL _C	(mol C) l ⁻¹
Ciliate nitrogen concentration	CIL _N	(mol N) l ⁻¹
Ciliate phosphate concentration	CIL _P	(mol P) l ⁻¹
Heterotrophic nanoflagellate cellular abundance	HNF	cell l ⁻¹
Heterotrophic nanoflagellate carbon concentration	HNF _C	(mol C) l ⁻¹
Heterotrophic nanoflagellate nitrogen concentration	HNF _N	(mol N) l ⁻¹
Heterotrophic nanoflagellate phosphate concentration	HNF _P	(mol P) l ⁻¹
Heterotrophic bacteria cellular abundance	BAC	cell l ⁻¹
Heterotrophic bacteria carbon concentration	BAC _C	(mol C) l ⁻¹
Heterotrophic bacteria nitrogen concentration	BAC _N	(mol N) l ⁻¹
Heterotrophic bacteria phosphate concentration	BAC _P	(mol P) l ⁻¹
Small phytoplankton cellular abundance	PHYS	(cell l ⁻¹
Small phytoplankton carbon concentration	PHYS _C	(mol C) l ⁻¹
Small phytoplankton chlorophyll concentration	PHYS _{CHL}	(g Chl) l ⁻¹
Small phytoplankton nitrogen concentration	PHYS _N	(mol N) l ⁻¹
Small phytoplankton phosphate concentration	PHYS _P	(mol P) l ⁻¹
Large phytoplankton cellular abundance	PHYL	cell l ⁻¹
Large phytoplankton carbon concentration	PHYL _C	(mol C) l ⁻¹
Large phytoplankton chlorophyll concentration	PHYL _{CHL}	(g Chl) l ⁻¹
Large phytoplankton nitrogen concentration	PHYL _N	(mol N) l ⁻¹
Large phytoplankton phosphate concentration	PHYL _P	(mol P) l ⁻¹
Nitrate concentration	NO3	(mol N) l ⁻¹
Ammonium concentration	NH4	(mol N) l ⁻¹
Phosphate concentration	PO4	(mol P) l ⁻¹
Labile dissolved organic carbon concentration	LDOC	(mol C) l ⁻¹
Semi-labile dissolved organic carbon concentration	SLDOC	(mol C) l ⁻¹
Labile dissolved organic nitrogen concentration	LDON	(mol N) l ⁻¹
Labile dissolved organic phosphate concentration	LDOP	(mol P) l ⁻¹
Large detrital particulate carbon concentration	DETL _C	(mol C) l ⁻¹
Large detrital particulate nitrogen concentration	DETL _N	(mol N) l ⁻¹
Large detrital particulate phosphate concentration	DETL _P	(mol P) l ⁻¹
Small detrital particulate carbon concentration	DETS _C	(mol C) l ⁻¹
Small detrital particulate nitrogen concentration	DETS _N	(mol N) l ⁻¹
Small detrital particulate phosphate concentration	DETS _P	(mol P) l ⁻¹

and arbitrarily distributed on three possible food, namely ciliates (30%), HNF (50%) and detrital material (20%), PHYL considered as being too large to be grazed by juveniles. Since Z

is only represented through an abundance and a carbon biomass, the N and P fluxes associated with the grazing by the juvenile Z are redirected to DETS.

A.2.3 Photosynthesis, Chlorophyll production and photoacclimation

The model uses Han (2002) mechanistic formulation for photosynthesis at steady state (see Baklouti et al. (2006b) for full details on this formulation and for the justification for the use of the steady-state version). In Han's model, each PSII is assumed to be in one of three possible states, namely open (i.e. reactive), closed (i.e. already activated), or photoinhibited. It also considers that the quantum yield of carbon fixation, and thus the specific primary production rate f_{nr}^{PP} , is proportional to the PSII probability of being open, and to the maximum quantum yield ϕ_{max}^C .

$$f_{nr}^{PP} = \frac{\phi_{max}^C \cdot \bar{a}^* \cdot E \cdot \theta}{1 + \sigma_{PSII} \cdot E \cdot \tau + (k_d^H/k_r) \cdot (\sigma_{PSII} \cdot E)^2 \cdot \tau} \quad (\text{A.4})$$

In Eq. A.4, \bar{a}^* stands for the spectrally-integrated Chl a-specific absorption coefficient over the [400–700] nm range, E for the irradiance, θ for the chlorophyll to carbon ratio, σ_{PSII} for the effective cross-section of PSII, τ for the turnover time of electron transfer, k_d^H for the dimensionless PSII damage rate, k_r for the PSII repair rate.

Chlorophyll synthesis has already been described in Eq. 9. The resulting plasticity of the Chl:C ratio allows the photoacclimation of phytoplankton under light-limited conditions. However, this photoacclimation proved to be insufficient in the case of very low light conditions as encountered in the region of deep chlorophyll maximum in the Eastern Mediterranean Basin. Using a function of irradiance (Eq. A.5) instead of a fixed value for the maximum Chl:C ratio θ_C^{\max} has partially solved this problem.

$$\theta_C^{\max} = 0.6 \cdot \exp(-0.3 \cdot E) + 0.6 \quad (\text{A.5})$$

A.2.4 Gross and net uptake

The gross uptake rate of nutrients or dissolved organic matter by phytoplankton or bacteria is classically represented through a Michaelis–Menten formulation:

$$f^{uptX} = V_X^{\max} \cdot \frac{[X]}{K_X + [X]}, \quad (\text{A.6})$$

where V_X^{\max} is the maximum uptake rate of element X and K_X the associated half-saturation constant. The inhibition of nitrate and DON uptake by ammonium and that of DOP by phosphate is also taken into account through the Harrison et al. (1996) formulation where $[INH]$ is the inhibitor's concentration and K_{INH} the inhibition constant. The specific uptake rate of a given element X in the presence of an inhibitor INH writes:

$$f^{uptX,INH} = V_X^{\max} \cdot \frac{[X]}{K_X + [X]} \cdot \frac{1}{1 + \frac{[INH]}{K_{INH}}} \quad (\text{A.7})$$

Finally, the feedback regulation of gross uptake of nutrients by the intracellular status of phytoplankton and bacteria has already been described in section 2.2.1.

A.2.5 Carbon net flux

Net carbon fluxes are calculated in the same way as nutrient net fluxes but with slight differences. Let us note F_{in} an inflow of carbon (either due to photosynthesis, grazing or DOC uptake) and proceeding at the specific rate r_C , the excess carbon outflow is calculated as follows:

- if $(Q_C^{PFT} \leq Q_C^{PFT, \min})$ or $(Q_C^{PFT} \geq Q_C^{PFT, \max})$, F_{net} and F_{out} are respectively given by Eqs. 6 and 5 in which $X=C$,
- else,

$$F_{out} = r_C \cdot \max(1 - h_{Q_C}, 1 - h_{Q_{NC}}, 1 - h_{Q_{PC}}) \cdot PFT_X \quad (A.8)$$

where h_{Q_C} is given by Eq. 2 in which C stands for X , and $h_{Q_{NC}}$ and $h_{Q_{PC}}$ are calculated according to A.9 in which Y either stands for N or P :

$$h_{Q_{YC}} = \left(\frac{Q_{YC} - Q_{YC}^{\min}}{Q_{YC}^{\max} - Q_{YC}^{\min}} \right)^{nn} \quad (A.9)$$

The value for nn exponent is set equal to 0.06 for heterotrophs and to 0.3 for autotrophs. The latter are indeed considered to have a different strategy than heterotrophs regarding carbon since it is provided by photosynthesis.

A.2.6 Grazing

The grazing specific rate is represented by a Holling II formulation (Holling, 1959) as revisited by (Kooijman, 2000):

$$f^{gPREY} = \frac{I_m [PREY]}{\frac{I_m}{F} + [PREY]} \quad (A.10)$$

where I_m is the maximum ingestion rate of the grazer, F either the clearance (for filter feeding organisms) or the attack rate, and $[PREY]_i$ the prey concentration of the prey (in cell l^{-1}).

It is generalized to several (here n_{prey}) preys using the “kill the winner”(KTW) formulation depicted in Vallina et al. (2014), which combines active switching (i.e., the preference of a predator for a given prey depends on prey density) and an ingestion rate always increasing with the total biomass of prey. This active-switching formulation was used to preserve food web diversity and to prevent unrealistic predator–prey oscillations. The variable prey preference (σ_i) for prey i due to active switching is defined as a function of the constant prey preference parameter for prey i (ϕ_i) as follows:

$$\sigma_i = \frac{\phi_i [PREY_i]}{\sum_{k=1}^{n_{prey}} [PREY_k]} \quad (A.11)$$

The grazing specific rate on prey i is given by:

$$f_g^{\text{PREY}_i} = \frac{\sigma_i F_i [\text{PREY}_i]}{\sum_{k=1}^{n_{\text{prey}}} \frac{\sigma_k F_k}{I_m^k} [\text{PREY}_k]} \cdot \frac{\left(\sum_{k=1}^{n_{\text{prey}}} \frac{\phi_k F_k}{I_m^k} [\text{PREY}_k] \right)^2}{1 + \left(\sum_{k=1}^{n_{\text{prey}}} \frac{\phi_k F_k}{I_m^k} [\text{PREY}_k] \right)^2} \quad (\text{A.12})$$

Finally, the feedback regulation of grazing fluxes by the internal status is achieved in the same way as for uptake regulation. For mesozooplankton, excess carbon will either be redirected towards LDOC (excretion, Eq. A.54) or DETL (faecal pellets, Eq. A.58). Moreover, since mesozooplankton is only represented in terms of an abundance and a C concentration (and not in N and P concentrations), the N and P fluxes associated with mesozooplankton grazing feed the DOX (N and P redirected fluxes in Eqs. A.56 and A.56) and DETS_X compartments (N and P redirected fluxes in Eqs. A.61 and A.62). For micro- and mesozooplankton, the excreted C, N and P fluxes feed the LDOC, NH₄ and PO₄ compartments, respectively.

A.2.7 Respiration

As in Baklouti et al. (2006b), the energy costs associated with the main phytoplankton activities have been included in the respiration term as follows:

$$f_{\text{PHY}}^{\text{resp}} = r_g f^{\text{PP}} + \sum_{\text{NUT}} r_{u_{\text{NUT}}} \cdot f_{\text{NUT}}^{\text{upt}} \cdot (1 - h_{Q_X}) \quad \text{where} \\ \text{NUT} \in \{\text{NO}_3, \text{NH}_4, \text{PO}_4\} \quad (\text{A.13})$$

r_g and $r_{u_{\text{NUT}}}$ respectively represent the cost associated with growth and uptake of nutrient NUT (see Tab. 6 for the units of these parameters).

The same is done for heterotrophic bacteria with DOM and DIM uptake:

$$f_{\text{BAC}}^{\text{resp}} = \sum_{\text{NUT}} r_{u_{\text{NUT}}} \cdot f_{\text{NUT}}^{\text{upt}} \cdot (1 - h_{Q_X}) \quad \text{where} \\ \text{NUT} \in \{\text{NO}_3, \text{NH}_4, \text{PO}_4, \text{DON}, \text{DOP}, \text{LDOC}, \text{SLDOC}\} \quad (\text{A.14})$$

Finally, zooplankton respiration is proportional to the net growth rate through:

$$f_{\text{ZOO}}^{\text{resp}} = r_g^z \cdot Q_C^{\text{ZOO}, \text{min}} \cdot f_{\text{ZOO}}^\mu \quad \text{where } \text{ZOO} \in \{\text{Z}, \text{CIL}, \text{HNF}\} \quad (\text{A.15})$$

A.2.8 Mortality

The specific rate of natural mortality is represented for a given PFT through a linear function which is applied not only to cellular abundances but to each concentration of this PFT:

$$f^m = k^m \quad (\text{A.16})$$

The model closure is achieved through a quadratic function implicitly representing the grazing pressure applied on mesozooplankton and large phytoplankton by higher trophic levels:

$$f^{mq} = k^{mq} \quad (\text{A.17})$$

A.2.9 Hydrolysis, mineralization and nitrification

In the model, large detrital particles (DETL) are hydrolysed into small detrital particles (DETS), and small detrital particles to dissolved organic matter (DOM). As for mineralization, the hydrolysis specific rate of a given detrital material DET_X ($X \in \{\text{N};\text{P}\}$) is a function of the carbon quota in bacteria:

$$f_{\text{BAC}}^{\text{hyd}_{\text{DET}_X}} = \frac{1}{86400 \tau_{\text{hyd}}} \cdot h_{Q_C}^{\text{BAC}} \quad (\text{A.18})$$

where τ_{hyd} is the turnover time of DET_X .

Moreover, based on the explanations provided in section 2.2 and on an outflow calculated with both quotas and ratio, the specific rate of mineralization of DOX (X either stands for N or P) into NH_4 and PO_4 writes:

$$f_{\text{BAC}}^{\text{rem}_{\text{DOX}}} = f_{\text{DOX}}^{\text{upt}} \cdot \max(1 - h_{Q_X}^{\text{BAC}}, 1 - h_{Q_{XC}}^{\text{BAC}}) \cdot h_{Q_C}^{\text{BAC}} \quad (\text{A.19})$$

$$f_{\text{BAC}}^{\text{out}_{\text{DOX}}} = f_{\text{DOX}}^{\text{upt}} \cdot \max(1 - h_{Q_X}^{\text{BAC}}, 1 - h_{Q_{XC}}^{\text{BAC}}) \cdot (1 - h_{Q_C}^{\text{BAC}}) \quad (\text{A.20})$$

Finally, concerning nitrification, it is described by a classical first order (i.e. linear) kinetics with τ^{nit} the nitrification rate constant, and writes:

$$f_{\text{NH}_4}^{\text{nit}} = \tau^{\text{nit}} \quad (\text{A.21})$$

All the functions used in the model are summarized in Tab. 2.

A.3 Model parameters and equations

A.3.1 Model functions

The name and the units of the mathematical functions included in the Eco3M-Med model are given in Tab. 2.

A.3.2 Model parameters

The model parameters for mesozooplankton, micro- and nanozooplankton, heterotrophic bacteria and phytoplankton are respectively given in Tabs. 3, 4, 5 and 6. Furthermore, some of the parameters are derived from a subset of reference parameters (see 2.3). Hence, Eq. A.22 relating the maximum uptake rate of a given element and the maximum specific growth rate

Table 2: *Mathematical functions involved in the model. The terms cell, pred and prey used in the units column respectively refer to a number of cells, a number of predators and a number of preys.*

Symbol	Definition	Units
f^μ	Specific growth rate	s^{-1}
f^{PChl}	Specific chlorophyll production rate	$\text{gChl cell}^{-1} s^{-1}$
f_{nr}^{PP}	Specific gross primary production rate (nutrient repleted)	s^{-1}
$f_{PFT}^{uptNUT_X}$	Specific gross uptake rate of nutrient NUT_X by PFT	$\text{mol X cell}^{-1} s^{-1}$
$f_{PFT}^{uptDOM_X}$	Specific gross uptake rate of DOM_X	$\text{mol X cell}^{-1} s^{-1}$
f_{PRED}^g	Specific grazing rate of PREY by PRED	$\text{prey pred}^{-1} s^{-1}$
f_Z^{gjuv}	Specific grazing rate by Z juveniles	$\text{mol C ind}^{-1} s^{-1}$
f^{resp}	Specific respiration rate	s^{-1}
f^{hyd}	Specific hydrolysis rate	s^{-1}
f^{rem}	Specific mineralization rate	$\text{mol X cell}^{-1} s^{-1}$
f_{NH4}^{nit}	Specific rate of nitrification	s^{-1}
f^m	Specific natural mortality rate	s^{-1}
f^{mq}	Specific quadratic mortality rate	$\text{cell (or ind.)}^{-1} m^3 s^{-1}$
h_{Q_X}	Quota function calculated with the X quota	–
$h_{Q_{XY}}$	Quota function calculated with the X:Y ratio	–
Q_X^{PFT}	Intracellular X quota in a given PFT	mol X cell^{-1} or mol X ind.^{-1}

conveys the fact that at steady-state and in nutrient-replete conditions, the maximum uptake rate of a given element should allow the population maximal growth to be sustained:

$$V_X^{\max} = \bar{\mu} \cdot Q_X^{\max} \quad (\text{A.22})$$

When nutrient concentration tends towards 0, the Michaëlis–Menten uptake rate should be proportional to the external diffusion of nutrients (both fluxes can actually not be equalized since they are not expressed in the same units (one being in $\text{mol cell}^{-1} s^{-1}$ and the other in mol s^{-1}), and due to the fact that the diffusion flux considers the whole cell surface while nutrient uptake only occurs on specific uptake sites. Furthermore, we consider in this new version that phytoplankton and bacteria are rather cigar-shaped (ellipsoid) than spherical. In such conditions, and considering the semiaxes a and b with $a^2 \gg b$, the diffusion flux writes (Kiorboe, 2008):

$$F_{\text{diff}} = \frac{4\pi D a X_\infty}{\ln\left(\frac{2a}{b}\right)} \quad (\text{A.23})$$

where D is the molecular diffusion coefficient of the nutrient and X_∞ its concentration in the medium (i.e. far from the cell surface). Posing $a = \frac{H}{2}$ and $b = \frac{a}{10}$, and considering that the uptake flux tends towards $\frac{V^{\max} X_\infty}{K_s}$ when $X_\infty \rightarrow 0$, one can write:

$$\frac{V^{\max}}{K_s} = A \cdot \frac{4\pi D H}{2 \ln(20)} \quad (\text{A.24})$$

where A , is a constant of proportionality, arbitrarily fixed to 1000 in order to obtain K_S values in a realistic order of magnitude (see Tables 5 and 6).

Table 3: *Model parameters for mesozooplankton (copepods).*

Symbol	Definition	Units	Value
Mesozooplankton			
<i>Individual contents and growth</i>			
$\bar{\mu}$	Maximum specific growth rate	s^{-1}	$0.5 \cdot 10^{-6}$
$Q_C^{Z,\min}$	Minimum carbon quota	mol ind^{-1}	$3 \cdot 10^{-7}$
$Q_C^{Z,\max}$	Maximum carbon quota	mol ind^{-1}	$7 \cdot 10^{-7}$
<i>Grazing</i>			
F	Clearance rate (prey1)	$\text{l pred}^{-1} \text{s}^{-1}$	$1.6 \cdot 10^{-5}$ (CIL)
F	Clearance rate (prey2)	$\text{l pred}^{-1} \text{s}^{-1}$	10^{-6} (HNF)
F	Clearance rate (prey3)	$\text{l pred}^{-1} \text{s}^{-1}$	$4 \cdot 10^{-6}$ (PHYL)
I_{MAX}	Max. ingestion rate (prey1)	$\text{prey pred}^{-1} \text{s}^{-1}$	0.05 (CIL)
I_{MAX}	Max. ingestion rate (prey2)	$\text{prey pred}^{-1} \text{s}^{-1}$	0.3 (HNF)
I_{MAX}	Max. ingestion rate (prey3)	$\text{prey pred}^{-1} \text{s}^{-1}$	0.18 (PHYL)
ϕ_1	Preference for (prey1)	–	0.35 (CIL)
ϕ_2	Preference for (prey2)	–	0.25 (HNF)
ϕ_3	Preference for (prey3)	–	0.4 (PHYL)
β_1	Preference of Z juvenile for CIL	–	0.3
β_2	Preference of Z juvenile for HNF	–	0.5
β_3	Preference of Z juvenile for DETS	–	0.2
<i>Mortality</i>			
k_m	Specific natural mortality rate	s^{-1}	$1.16 \cdot 10^{-7}$
k_{mq}	Specific quadratic mortality rate	$\text{ind}^{-1} \text{l s}^{-1}$	$1 \cdot 10^{-7}$
<i>Respiration and excretion</i>			
r_g	Energetic cost for growth (Eq. A.15)	–	$3 \cdot 10^{-7}$
<i>Others</i>			
ϵ	Proportion of released flow to faecal pellets	–	0.3
β	Redirection of N and P grazing fluxes towards DET	–	0.1
γ	Proportion of lost food due to sloppy feeding	–	0.1

Table 4: *Model parameters for micro- and nanozooplankton. Parameter values have been taken from Perez et al. (1997); Sherr et al. (1989); Christaki et al. (1999) for ciliates, and from Christaki et al. (1999, 2009) for HNF, or have been derived from other parameters.*

Symbol	Definition	Units	Value CIL	Value HNF
<i>Nano- and microzooplankton</i>				
<i>Intracellular quotas and growth</i>				
$\bar{\mu}$	Maximum specific growth rate	s^{-1}	$1.25 \cdot 10^{-5}$	$2.05 \cdot 10^{-5}$
Q_P^{min}	Minimum phosphate quota	mol cell^{-1}	$1.27 \cdot 10^{-12}$	$1.15 \cdot 10^{-15}$
Q_P^{max}	Maximum phosphate quota	mol cell^{-1}	$3 Q_P^{min}$	$3 Q_P^{min}$
Q_N^{min}	Minimum nitrogen quota	mol cell^{-1}	$2.03 \cdot 10^{-11}$	$1.84 \cdot 10^{-14}$
Q_N^{max}	Maximum nitrogen quota	mol cell^{-1}	$3 Q_N^{min}$	$3 Q_N^{min}$
Q_C^{min}	Minimum carbon quota	mol cell^{-1}	$1.35 \cdot 10^{-10}$	$1.22 \cdot 10^{-13}$
Q_C^{max}	Maximum carbon quota	mol cell^{-1}	$3 Q_C^{min}$	$3 Q_C^{min}$
Q_{CN}^{min}	Minimum C:N ratio in Zoo.	mol mol^{-1}	Q_C^{min} / Q_N^{max}	Q_C^{min} / Q_N^{max}
Q_{CN}^{max}	Maximum C:N ratio in Zoo.	mol mol^{-1}	Q_C^{max} / Q_N^{min}	Q_C^{max} / Q_N^{min}
Q_{CP}^{min}	Minimum C:P ratio in Zoo.	mol mol^{-1}	Q_C^{min} / Q_P^{max}	Q_C^{min} / Q_P^{max}
Q_{CP}^{max}	Maximum C:P ratio in Zoo.	mol mol^{-1}	Q_C^{max} / Q_P^{min}	Q_C^{max} / Q_P^{min}
<i>Grazing</i>				
F	Clearance rate (prey1)	$\text{l ind}^{-1} \text{s}^{-1}$	10^{-9} (HNF)	$0.1 \cdot 10^{-10}$ (PHYS)
F	Clearance rate (prey2)	$\text{l ind}^{-1} \text{s}^{-1}$	$6.25 \cdot 10^{-9}$ (PHYS)	$5 \cdot 10^{-12}$ (BAC)
F	Clearance rate (prey3)	$\text{l ind}^{-1} \text{s}^{-1}$	$6.25 \cdot 10^{-9}$ (BAC)	–
I_{MAX}	Max. ingestion rate (prey1)	$\text{ind ind}^{-1} \text{s}^{-1}$	$7 \cdot 10^{-3}$ (HNF)	10^{-4} (PHYS)
I_{MAX}	Max. ingestion rate (prey2)	$\text{ind ind}^{-1} \text{s}^{-1}$	$8 \cdot 10^{-2}$ (PHYS)	10^{-3} (BAC)
I_{MAX}	Max. ingestion rate (prey3)	$\text{ind ind}^{-1} \text{s}^{-1}$	0.4 (BAC)	–
ϕ_1	Preference for (prey1)	–	0.65 (HNF)	0.3 (PHYS)
ϕ_2	Preference for (prey2)	–	0.2 (PHYS)	0.7 (BAC)
ϕ_3	Preference for (prey3)	–	0.15 (BAC)	–
r_g	Energetic cost for growth (Eq. A.15)	–	$1.3 \cdot 10^{-11}$	$1.2 \cdot 10^{-14}$
<i>Mortality</i>				
k_m	Specific natural mortality rate	s^{-1}	$1.16 \cdot 10^{-6}$	$1.16 \cdot 10^{-6}$

Table 5: Model parameters for heterotrophic bacteria. Parameter values are either taken from Thingstad (2005), Guyennon et al. (2015), Mauriac et al. (2011) and references herein, or calculated from other parameters. D_{NO_3} , D_{NH_4} , D_{PO_4} , D_{DON} , D_{DOP} are the diffusion coefficient of NO_3 , NH_4 , PO_4 , DON and DOP , respectively equal to $1.7 \cdot 10^{-9}$, $1.9 \cdot 10^{-9}$, $7.5 \cdot 10^{-10}$, $3 \cdot 10^{-10}$, $3 \cdot 10^{-10} \text{ m}^2 \text{ s}^{-1}$.

Symbol	Definition	Units	Value
Heterotrophic bacteria			
<i>Intracellular quotas and growth</i>			
$\bar{\mu}$	Maximum specific growth rate	s^{-1}	$3.6 \cdot 10^{-5}$
Q_P^{\min}	Minimum phosphate quota	mol cell^{-1}	$7.6 \cdot 10^{-18}$
Q_P^{\max}	Maximum phosphate quota	mol cell^{-1}	$3 Q_P^{\min}$
Q_N^{\min}	Minimum nitrogen quota	mol cell^{-1}	$1.21 \cdot 10^{-16}$
Q_N^{\max}	Maximum nitrogen quota	mol cell^{-1}	$3 Q_N^{\min}$
Q_C^{\min}	Minimum carbon quota	mol cell^{-1}	$8.06 \cdot 10^{-16}$
Q_C^{\max}	Maximum carbon quota	mol cell^{-1}	$3 Q_C^{\min}$
Q_{CN}^{\min}	Minimum C:N ratio in bac.	mol mol^{-1}	Q_C^{\min} / Q_N^{\max}
Q_{CN}^{\max}	Maximum C:N ratio in bac.	mol mol^{-1}	Q_C^{\max} / Q_N^{\min}
Q_{CP}^{\min}	Minimum C:P ratio in bac.	mol mol^{-1}	Q_C^{\min} / Q_P^{\max}
Q_{CP}^{\max}	Maximum C:P ratio in bac.	mol mol^{-1}	Q_C^{\max} / Q_P^{\min}
<i>Nutrient uptake</i>			
H	Major axis of the cigar-shaped cells	μm	0.8
V_N^{\max}	Maximum uptake rate for NH_4 , NO_3 and DON	$\text{mol N cell}^{-1} \text{ s}^{-1}$	$\bar{\mu} \cdot Q_N^{\max}$
K_{NH_4}	Half-saturation constant for NH_4 uptake	mol N l^{-1}	Eq. A.24 using D_{NH_4}
K_{NO_3}	Half-saturation constant for NO_3 uptake	mol N l^{-1}	Eq. A.24 using D_{NO_3}
K_{DON}	Half-saturation constant for DON	mol N l^{-1}	Eq. A.24 using D_{DON}
V_P^{\max}	Maximum uptake rate for PO_4	$\text{mol P cell}^{-1} \text{ s}^{-1}$	$\bar{\mu} \cdot Q_P^{\max}$
K_{PO_4}	Half-saturation constant for PO_4 uptake	mol P l^{-1}	Eq. A.24 using D_{PO_4}
K_{DOP}	Half-saturation constant for DOP	mol P l^{-1}	Eq. A.24 using D_{DOP}
$K_{inh}^{NO_3}$	Inhibition of nitrate uptake by ammonium	mol l^{-1}	$5 \cdot 10^{-6}$
K_{inh}^{DON}	Inhibition of DON uptake by ammonium	mol l^{-1}	$5 \cdot 10^{-6}$
K_{inh}^{DOP}	Inhibition of DOP uptake by Phosphate	mol l^{-1}	$5 \cdot 10^{-6}$
V_{LDOC}^{\max}	Maximum uptake rate for $LDOC$ and $SLDOC$	$\text{mol cell}^{-1} \text{ s}^{-1}$	$\bar{\mu} \cdot Q_C^{\max}$
K_{LDOC}	Half-saturation constant for $LDOC$	mol l^{-1}	$4 \cdot 10^{-7}$
K_{SLDOC}	Half-saturation constant for $SLDOC$	mol l^{-1}	$1 \cdot 10^{-5}$
<i>Respiration</i>			
r_{uDON}	Energetic cost for the uptake of DON	$(\text{mol C}) (\text{mol N})^{-1}$	0.397
r_{uDOP}	Energetic cost for the uptake of DOP	$(\text{mol C}) (\text{mol P})^{-1}$	0.155
r_{uLDOC}	Energetic cost for the uptake of $LDOC$	–	0.15
r_{uSLDOC}	Energetic cost for the uptake of $SLDOC$	–	0.25
<i>Hydrolysis and nitrification</i>			
τ_{hyd}^{DETS}	Turnover time for the hydrol. of $DETS$	d	7.5
τ_{hyd}^{DETL}	Turnover time for the hydrol. of $DETL$	d	4.5
τ^{nit}	Nitrification rate constant	s^{-1}	$3 \cdot 10^{-5}$
<i>Mortality</i>			
k_m	Specific natural mortality rate	s^{-1}	$1.16 \cdot 10^{-6}$

Table 6: *Model parameters for phytoplankton. Parameter values are either taken from Thingstad (2005), Han (2002), Baklouti et al. (2006b), Guyennon et al. (2015), Mauriac et al. (2011) and references herein, or calculated from other parameters. D_{NO_3} , D_{NH_4} , D_{PO_4} , D_{DON} , D_{DOP} are the diffusion coefficient of NO_3 , NH_4 , PO_4 , DON and DOP , respectively equal to $1.7 \cdot 10^{-9}$, $1.9 \cdot 10^{-9}$, $7.5 \cdot 10^{-10}$, $3 \cdot 10^{-10}$, $3 \cdot 10^{-10} \text{ m}^2 \text{ s}^{-1}$.*

Symbol	Definition	Units	Value PHYL	Value PHYS
Phytoplankton				
<i>Intracellular quotas and growth</i>				
$\bar{\mu}$	Maximum specific growth rate	s^{-1}	$2.3 \cdot 10^{-5}$	$3.2 \cdot 10^{-5}$
Q_P^{\min}	Minimum phosphate quota	mol cell^{-1}	$2.15 \cdot 10^{-14}$	$6.45 \cdot 10^{-17}$
Q_P^{\max}	Maximum phosphate quota	mol cell^{-1}	$3 Q_P^{\min}$	$3 Q_P^{\min}$
Q_N^{\min}	Minimum nitrogen quota	mol cell^{-1}	$3.44 \cdot 10^{-13}$	$1.03 \cdot 10^{-15}$
Q_N^{\max}	Maximum nitrogen quota	mol cell^{-1}	$3 Q_N^{\min}$	$3 Q_N^{\min}$
Q_C^{\min}	Minimum carbon quota	mol cell^{-1}	$2.27 \cdot 10^{-12}$	$6.83 \cdot 10^{-15}$
Q_C^{\max}	Maximum carbon quota	mol cell^{-1}	$3 Q_C^{\min}$	$3 Q_C^{\min}$
Q_{CN}^{\min}	Minimum C:N ratio in phy.	mol mol^{-1}	Q_C^{\min}/Q_N^{\max}	Q_C^{\min}/Q_N^{\max}
Q_{CN}^{\max}	Maximum C:N ratio in phy.	mol mol^{-1}	Q_C^{\max}/Q_N^{\min}	Q_C^{\max}/Q_N^{\min}
Q_{CP}^{\min}	Minimum C:P ratio in phy.	mol mol^{-1}	Q_C^{\min}/Q_P^{\max}	Q_C^{\min}/Q_P^{\max}
Q_{CP}^{\max}	Maximum C:P ratio in phy.	mol mol^{-1}	Q_C^{\max}/Q_P^{\min}	Q_C^{\max}/Q_P^{\min}
<i>Nutrient uptake</i>				
H	Major axis of the cigar-shaped cells	μm	40	5
V_N^{\max}	Maximum uptake rate for NO_3 , NH_4 and DON	$\text{mol cell}^{-1} \text{ s}^{-1}$	$\bar{\mu} \cdot Q_N^{\max}$	$\bar{\mu} \cdot Q_N^{\max}$
K_{NH_4}	Half-saturation constant for NH_4	mol l^{-1}	Eq. A.24 using D_{NH_4}	
K_{NO_3}	Half-saturation constant for NO_3	mol l^{-1}	Eq. A.24 using D_{NO_3}	
K_{DON}	Half-saturation constant for DON	mol l^{-1}	–	Eq. A.24
V_P^{\max}	Maximum uptake rate for PO_4 and DOP	$\text{mol cell}^{-1} \text{ s}^{-1}$	$\bar{\mu} \cdot Q_P^{\max}$	$\bar{\mu} \cdot Q_P^{\max}$
K_{PO_4}	Half-saturation constant for PO_4	mol l^{-1}	Eq. A.24 using D_{PO_4}	
K_{DOP}	Half-saturation constant for DOP	mol l^{-1}	Eq. A.24 using D_{DOP}	
$K_{inh}^{NO_3}$	Inhibition of nitrate uptake by NH_4	mol l^{-1}	10^{-3}	10^{-6}
K_{inh}^{DON}	Inhibition of DON uptake by NH_4	mol l^{-1}	–	$5 \cdot 10^{-6}$
K_{inh}^{DOP}	Inhibition of DOP uptake by PO_4	mol l^{-1}	$5 \cdot 10^{-6}$	$5 \cdot 10^{-6}$
<i>Photosynthesis and respiration</i>				
τ	Electron turnover-time in PSII	s	$1.8 \cdot 10^{-3}$	$1.3 \cdot 10^{-3}$
σ_{PSII}	PSII cross section	$\text{m}^2 \text{ J}^{-1}$	2.5	2
k_d^H	Dimensionless rate of PSII damage	–	$4.5 \cdot 10^{-8}$	$4.5 \cdot 10^{-8}$
k_r	PSII repair rate	s^{-1}	$2.6 \cdot 10^{-4}$	$2.6 \cdot 10^{-4}$
\bar{a}^*	Mean Chl a -specific absorption coefficient	$\text{m}^2 \text{ gChl}^{-1}$	8	14
ϕ_{max}^C	Max. quantum yield for carbon fixation	mol C J^{-1}	$2.3 \cdot 10^{-7}$	$1.25 \cdot 10^{-7}$
θ_N^{\max}	Max. Chl:N ratio	gChl mol N^{-1}	2.7	2.3
θ_C^{\max}	Maximum Chl:C ratio	gChl mol C^{-1}	Eq. A.5	Eq. A.5
r_g	Cost for primary production	–	0.25	0.1
r_{uNO_3}	Cost of nitrate uptake	$(\text{mol C}) (\text{mol N})^{-1}$	0.397	0.397
r_{uNH_4}	Cost of ammonium uptake	$(\text{mol C}) (\text{mol N})^{-1}$	0.198	0.198
r_{uPO_4}	Cost of phosphate uptake	$(\text{mol C}) (\text{mol P})^{-1}$	0.155	0.155
<i>Mortality</i>				
k_m	Specific natural mortality rate	s^{-1}	$1.16 \cdot 10^{-6}$	$8.16 \cdot 10^{-7}$
k_{mq}	Specific quadratic mortality rate	$\text{cell}^{-1} \text{ l s}^{-1}$	$6.7 \cdot 10^{-13}$	–

A.3.3 Model equations

Mesozooplankton (adults)

$$\frac{dZ}{dt} = \underbrace{f_z^\mu \cdot Z}_{\text{growth}} - \underbrace{f_z^m \cdot Z}_{\text{nat. mortality}} - \underbrace{f_z^{mq} \cdot Z^2}_{\text{grazing by higher trophic levels}} \quad (\text{A.25})$$

$$\begin{aligned} \frac{dZ_C}{dt} &= \underbrace{(f_z^{g^{\text{CIL}}} \cdot Q_C^{\text{CIL}} + f_z^{g^{\text{HNF}}} \cdot Q_C^{\text{HNF}} + f_z^{g^{\text{PHYL}}} \cdot Q_C^{\text{PHYL}})}_{\text{net grazing on CIL, HNF and PHYL}} \cdot h_{Q_C^Z} \cdot Z \\ &- \underbrace{f_z^{\text{resp}} \cdot Z_C}_{\text{respiration}} - \underbrace{f_z^m \cdot Z_C}_{\text{nat. mortality}} - \underbrace{f_z^{mq} \cdot Z^2 \cdot Q_C^Z}_{\text{grazing by high. troph. lev.}} \\ &+ \underbrace{(\beta_1 \cdot f_z^{g^{\text{CIL}}} + \beta_2 \cdot f_z^{g^{\text{HNF}}} + \beta_3 \cdot f_z^{g^{\text{POC}}}) \cdot Z}_{\text{feeding during juvenilestages on CIL, HNF and DETS}} \end{aligned} \quad (\text{A.26})$$

Microzooplankton

$$\frac{d\text{CIL}}{dt} = \underbrace{f_{\text{CIL}}^\mu \cdot \text{CIL}}_{\text{growth}} - \underbrace{f_{\text{CIL}}^m \cdot \text{CIL}}_{\text{nat. mortality}} - \underbrace{f_z^{g^{\text{CIL}}} \cdot Z}_{\text{grazing by Z}} - \underbrace{\beta_1 \cdot f_z^{g^{\text{CIL}}} \cdot \frac{Z}{Q_C^{\text{CIL}}}}_{\text{grazing by Z during juvenile stages}} \quad (\text{A.27})$$

$$\begin{aligned} \frac{d\text{CIL}_C}{dt} &= \underbrace{(f_{\text{CIL}}^{g^{\text{HNF}}} \cdot Q_C^{\text{HNF}} + f_{\text{CIL}}^{g^{\text{PHYS}}} \cdot Q_C^{\text{PHYS}} + f_{\text{CIL}}^{g^{\text{BAC}}} \cdot Q_C^{\text{BAC}})}_{\text{net grazing on HNF and PHYS and BAC}} \cdot h_{Q_C^{\text{CIL}}} \cdot \text{CIL} \\ &- \underbrace{f_{\text{CIL}}^{\text{resp}} \cdot \text{CIL}_C}_{\text{respiration}} - \underbrace{f_{\text{CIL}}^m \cdot \text{CIL}_C}_{\text{nat. mort.}} - \underbrace{f_z^{g^{\text{CIL}}} \cdot Q_C^{\text{CIL}} \cdot Z}_{\text{grazing by Z}} - \underbrace{\beta_1 \cdot f_z^{g^{\text{CIL}}} \cdot Z}_{\text{grazing by Z during juvenile stages}} \end{aligned} \quad (\text{A.28})$$

$$\begin{aligned} \frac{d\text{CIL}_N}{dt} &= \underbrace{f_{\text{CIL}}^{g^{\text{HNF}}} \cdot h_{Q_N^{\text{CIL}}} \cdot Q_N^{\text{HNF}} \cdot \text{CIL}}_{\text{feeding on HNF}} + \underbrace{f_{\text{CIL}}^{g^{\text{PHYS}}} \cdot h_{Q_N^{\text{CIL}}} \cdot Q_N^{\text{PHYS}} \cdot \text{CIL}}_{\text{grazing on PHYS}} \\ &+ \underbrace{f_{\text{CIL}}^{g^{\text{BAC}}} \cdot h_{Q_N^{\text{CIL}}} \cdot Q_N^{\text{BAC}} \cdot \text{CIL}}_{\text{feeding on BAC}} - \underbrace{f_{\text{CIL}}^m \cdot \text{CIL}_N}_{\text{nat. mortality}} - \underbrace{f_z^{g^{\text{CIL}}} \cdot Q_N^{\text{CIL}} \cdot Z}_{\text{grazing by Z}} \\ &- \underbrace{\beta_1 \cdot f_z^{g^{\text{CIL}}} \cdot Z \cdot \frac{Q_N^{\text{CIL}}}{Q_C^{\text{CIL}}}}_{\text{grazing by Z during juvenile stages}} \end{aligned} \quad (\text{A.29})$$

$$\begin{aligned} \frac{d\text{CIL}_P}{dt} &= \underbrace{f_{\text{CIL}}^{g^{\text{HNF}}} \cdot h_{Q_P^{\text{CIL}}} \cdot Q_P^{\text{HNF}} \cdot \text{CIL}}_{\text{feeding on HNF}} + \underbrace{f_{\text{CIL}}^{g^{\text{PHYS}}} \cdot h_{Q_P^{\text{CIL}}} \cdot Q_P^{\text{PHYS}} \cdot \text{CIL}}_{\text{feeding on PHYS}} \\ &+ \underbrace{f_{\text{CIL}}^{g^{\text{BAC}}} \cdot h_{Q_P^{\text{CIL}}} \cdot Q_P^{\text{BAC}} \cdot \text{CIL}}_{\text{feeding on BAC}} - \underbrace{f_{\text{CIL}}^m \cdot \text{CIL}_P}_{\text{nat. mortality}} - \underbrace{f_z^{g^{\text{CIL}}} \cdot Q_P^{\text{CIL}} \cdot Z}_{\text{grazing by Z}} \\ &- \underbrace{\beta_1 \cdot f_z^{g^{\text{CIL}}} \cdot Z \cdot \frac{Q_P^{\text{CIL}}}{Q_C^{\text{CIL}}}}_{\text{grazing by Z during juvenile stages}} \end{aligned} \quad (\text{A.30})$$

Nanozooplankton

$$\begin{aligned} \frac{d\text{HNF}}{dt} &= \underbrace{f_{\text{HNF}}^{\mu} \cdot \text{HNF}}_{\text{growth}} - \underbrace{f_{\text{HNF}}^m \cdot \text{HNF}}_{\text{nat. mortality}} - \underbrace{f_z^{g\text{HNF}} \cdot Z - f_{\text{CIL}}^{g\text{HNF}} \cdot \text{CIL}}_{\text{grazing by Z and CIL}} \\ &- \underbrace{\beta_2 \cdot f_z^{g\text{HNF}} \frac{Z}{Q_C^{\text{HNF}}}}_{\substack{\text{grazing by Z} \\ \text{during juv. stages}}} \end{aligned} \quad (\text{A.31})$$

$$\begin{aligned} \frac{d\text{HNF}_C}{dt} &= \underbrace{(f_{\text{HNF}}^{g\text{PHYS}} \cdot Q_C^{\text{PHYS}} + f_{\text{HNF}}^{g\text{BAC}} \cdot Q_C^{\text{BAC}}) \cdot h_{Q_C}^{\text{HNF}} \cdot \text{HNF}}_{\text{feeding on PHYS and BAC}} - \underbrace{f_{\text{HNF}}^{\text{resp}} \cdot \text{HNF}_C}_{\text{respiration}} \\ &- \underbrace{f_{\text{HNF}}^m \cdot \text{HNF}_C}_{\text{nat. mortality}} - \underbrace{f_z^{g\text{HNF}} \cdot Q_C^{\text{HNF}} \cdot Z}_{\text{grazing by Z}} - \underbrace{f_{\text{CIL}}^{g\text{HNF}} \cdot Q_C^{\text{HNF}} \cdot \text{CIL}}_{\text{grazing by CIL}} \\ &- \underbrace{\beta_2 \cdot f_z^{g\text{HNF}} \cdot Z}_{\text{grazing by Z during juvenile stages}} \end{aligned} \quad (\text{A.32})$$

$$\begin{aligned} \frac{d\text{HNF}_N}{dt} &= \underbrace{(f_{\text{HNF}}^{g\text{PHYS}} \cdot Q_N^{\text{PHYS}} + f_{\text{HNF}}^{g\text{BAC}} \cdot Q_N^{\text{BAC}}) \cdot h_{Q_N}^{\text{HNF}} \cdot \text{HNF}}_{\text{grazing on PHYS and BAC}} - \underbrace{f_{\text{HNF}}^m \cdot \text{HNF}_N}_{\text{nat. mortality}} \\ &- \underbrace{(f_z^{g\text{HNF}} \cdot Z + f_{\text{CIL}}^{g\text{HNF}} \cdot \text{CIL}) \cdot Q_N^{\text{HNF}}}_{\text{grazing by Z and CIL}} - \underbrace{\beta_2 \cdot f_z^{g\text{HNF}} \cdot Z \cdot \frac{Q_N^{\text{HNF}}}{Q_C^{\text{HNF}}}}_{\substack{\text{grazing by Z} \\ \text{during juvenile stages}}} \end{aligned} \quad (\text{A.33})$$

$$\begin{aligned} \frac{d\text{HNF}_P}{dt} &= \underbrace{(f_{\text{HNF}}^{g\text{PHYS}} \cdot Q_P^{\text{PHYS}} + f_{\text{HNF}}^{g\text{BAC}} \cdot Q_P^{\text{BAC}}) \cdot h_{Q_P}^{\text{HNF}} \cdot \text{HNF}}_{\text{grazing on PHYS and BAC}} - \underbrace{f_{\text{HNF}}^m \cdot \text{HNF}_P}_{\text{nat. mortality}} \\ &- \underbrace{(f_z^{g\text{HNF}} \cdot Z + f_{\text{CIL}}^{g\text{HNF}} \cdot \text{CIL}) \cdot Q_P^{\text{HNF}}}_{\text{grazing by Z and CIL}} - \underbrace{\beta_2 \cdot f_z^{g\text{HNF}} \cdot Z \cdot \frac{Q_P^{\text{HNF}}}{Q_C^{\text{HNF}}}}_{\substack{\text{grazing by Z} \\ \text{during juvenile stages}}} \end{aligned} \quad (\text{A.34})$$

Bacteria

$$\frac{d\text{BAC}}{dt} = \underbrace{f_{\text{BAC}}^{\mu} \cdot \text{BAC}}_{\text{growth}} - \underbrace{f_{\text{BAC}}^m \cdot \text{BAC}}_{\text{nat. mortality}} - \underbrace{f_{\text{HNF}}^{g\text{BAC}} \cdot \text{HNF}}_{\text{grazing by HNF}} - \underbrace{f_{\text{CIL}}^{g\text{BAC}} \cdot \text{CIL}}_{\text{grazing by CIL}} \quad (\text{A.35})$$

$$\begin{aligned} \frac{d\text{BAC}_C}{dt} &= \underbrace{(f_{\text{BAC}}^{\text{uptLDOC}} + f_{\text{BAC}}^{\text{uptSLDOC}}) \cdot h_{Q_C}^{\text{BAC}} \cdot \text{BAC}}_{\text{net uptake of LDOC and SLDOC}} - \underbrace{f_{\text{BAC}}^{\text{resp}} \cdot \text{BAC}}_{\text{respiration and uptake cost}} \\ &- \underbrace{f_{\text{BAC}}^m \cdot \text{BAC}_C}_{\text{nat. mortality}} - \underbrace{f_{\text{HNF}}^{g\text{BAC}} \cdot Q_C^{\text{BAC}} \cdot \text{HNF}}_{\text{grazing by HNF}} - \underbrace{f_{\text{CIL}}^{g\text{BAC}} \cdot Q_C^{\text{BAC}} \cdot \text{CIL}}_{\text{grazing by CIL}} \end{aligned} \quad (\text{A.36})$$

$$\begin{aligned} \frac{d\text{BAC}_N}{dt} &= \underbrace{f_{\text{BAC}}^{\text{uptN}} \cdot h_{Q_N}^{\text{BAC}} \cdot \text{BAC}}_{\text{net uptake of N}} - \underbrace{f_{\text{BAC}}^m \cdot \text{BAC}_N}_{\text{nat. mortality}} - \underbrace{f_{\text{HNF}}^{g\text{BAC}} \cdot Q_N^{\text{BAC}} \cdot \text{HNF}}_{\text{grazing by HNF}} \\ &- \underbrace{f_{\text{CIL}}^{g\text{BAC}} \cdot Q_N^{\text{BAC}} \cdot \text{CIL}}_{\text{grazing by CIL}} \end{aligned} \quad (\text{A.37})$$

$$\begin{aligned} \frac{d\text{BAC}_P}{dt} &= \underbrace{f_{\text{BAC}}^{\text{uptP}} \cdot h_{Q_P}^{\text{BAC}} \cdot \text{BAC}}_{\text{net uptake of P}} - \underbrace{f_{\text{BAC}}^m \cdot \text{BAC}_P}_{\text{nat. mortality}} - \underbrace{f_{\text{HNF}}^{g\text{BAC}} \cdot Q_P^{\text{BAC}} \cdot \text{HNF}}_{\text{grazing by HNF}} \\ &- \underbrace{f_{\text{CIL}}^{g\text{BAC}} \cdot Q_P^{\text{BAC}} \cdot \text{CIL}}_{\text{grazing by CIL}} \end{aligned} \quad (\text{A.38})$$

Phytoplankton

$$\frac{d\text{PHYL}}{dt} = \underbrace{f_{\text{PHYL}}^{\mu} \cdot \text{PHYL}}_{\text{growth}} - \underbrace{f_{\text{PHYL}}^m \cdot \text{PHYL}}_{\text{nat. mortality}} - \underbrace{f_Z^{g\text{PHYL}} \cdot Z}_{\text{graz. by Z}} - \underbrace{f_{\text{PHYL}}^{mq} \cdot \text{PHYL}^2}_{\text{grazing by higher trophic levels}} \quad (\text{A.39})$$

$$\begin{aligned} \frac{d\text{PHYLC}}{dt} &= \underbrace{f_{nr}^{\text{PP}} \cdot h_{Q_C}^{\text{PHYL}} \cdot \text{PHYLC}}_{\text{primary production}} - \underbrace{f_{\text{PHYL}}^{\text{resp}} \cdot \text{PHYLC}}_{\text{resp. and uptake cost}} - \underbrace{f_{\text{PHYL}}^m \cdot \text{PHYLC}}_{\text{nat. mortality}} \quad (\text{A.40}) \\ &- \underbrace{f_Z^{g\text{PHYL}} \cdot Q_C^{\text{PHYL}} \cdot Z}_{\text{grazing by Z}} - \underbrace{f_{\text{PHYL}}^{mq} \cdot \text{PHYLC}^2 \cdot Q_C^{\text{PHYL}}}_{\text{grazing by higher trophic levels}} \end{aligned}$$

$$\begin{aligned} \frac{d\text{PHYLN}}{dt} &= \underbrace{f_{\text{PHYL}}^{\text{uptN}} \cdot h_{Q_N}^{\text{PHYL}} \cdot \text{PHYLN}}_{\text{uptake}} - \underbrace{f_{\text{PHYL}}^m \cdot \text{PHYLN}}_{\text{nat. mortality}} \quad (\text{A.41}) \\ &- \underbrace{f_Z^{g\text{PHYL}} \cdot Z \cdot Q_N^{\text{PHYL}}}_{\text{grazing by Z}} - \underbrace{f_{\text{PHYL}}^{mq} \cdot \text{PHYLN}^2 \cdot Q_N^{\text{PHYL}}}_{\text{grazing by higher trop. levels}} \end{aligned}$$

$$\begin{aligned} \frac{d\text{PHYLP}}{dt} &= \underbrace{f_{\text{PHYL}}^{\text{uptP}} \cdot h_{Q_P}^{\text{PHYL}} \cdot \text{PHYLP}}_{\text{uptake}} - \underbrace{f_{\text{PHYL}}^m \cdot \text{PHYLP}}_{\text{nat. mortality}} \quad (\text{A.42}) \\ &- \underbrace{f_Z^{g\text{PHYL}} \cdot Q_P^{\text{PHYL}} \cdot Z}_{\text{grazing by Z}} - \underbrace{f_{\text{PHYL}}^{mq} \cdot \text{PHYLP}^2 \cdot Q_P^{\text{PHYL}}}_{\text{grazing by higher trophic levels}} \end{aligned}$$

$$\begin{aligned} \frac{d\text{PHYL}_{\text{CHL}}}{dt} &= \underbrace{f^{P\text{Chl}} \cdot \text{PHYL}}_{\text{chlorophyll synthesis}} - \underbrace{f_{\text{PHYL}}^m \cdot \text{PHYL}_{\text{CHL}}}_{\text{nat. mortality}} - \underbrace{f_Z^{g\text{PHYL}} \cdot Q_{\text{CHL}}^{\text{PHYL}} \cdot Z}_{\text{grazing by Z}} \quad (\text{A.43}) \\ &- \underbrace{f_{\text{PHYL}}^{mq} \cdot \text{PHYL}^2 \cdot \theta_C^{\text{PHYL}}}_{\text{grazing by higher trophic levels}} \end{aligned}$$

$$f_{\text{PHYL}}^{\text{uptN}} = f_{\text{PHYL}}^{\text{uptNO}_3} + f_{\text{PHYL}}^{\text{uptNH}_4} \quad (\text{A.44})$$

$$f_{\text{PHYL}}^{\text{uptP}} = f_{\text{PHYL}}^{\text{uptPO}_4} + f_{\text{PHYL}}^{\text{uptDOP}} \quad (\text{A.45})$$

$$\frac{d\text{PHYS}}{dt} = \underbrace{f_{\text{PHYS}}^{\mu} \cdot \text{PHYS}}_{\text{growth}} - \underbrace{f_{\text{PHYS}}^m \cdot \text{PHYS}}_{\text{nat. mort.}} - \underbrace{f_{\text{CIL}}^{g^{\text{PHYS}}} \cdot \text{CIL}}_{\text{graz. by CIL}} - \underbrace{f_{\text{HNF}}^{g^{\text{PHYS}}} \cdot \text{HNF}}_{\text{graz. by HNF}} \quad (\text{A.46})$$

$$\begin{aligned} \frac{d\text{PHYS}_C}{dt} &= \underbrace{f_{\text{nr}}^{\text{PP}} \cdot h_{Q_C}^{\text{PHYS}} \cdot \text{PHYS}_C}_{\text{primary production}} - \underbrace{f_{\text{PHYS}}^{\text{resp}} \cdot \text{PHYS}_C}_{\text{respiration and uptake cost}} \\ &- \underbrace{f_{\text{PHYS}}^m \cdot \text{PHYS}_C}_{\text{nat. mortality}} - \underbrace{(f_{\text{CIL}}^{g^{\text{PHYS}}} \cdot \text{CIL} + f_{\text{HNF}}^{g^{\text{PHYS}}} \cdot \text{HNF}) \cdot Q_C^{\text{PHYS}}}_{\text{grazing by CIL and HNF}} \end{aligned} \quad (\text{A.47})$$

$$\begin{aligned} \frac{d\text{PHYS}_N}{dt} &= \underbrace{f_{\text{PHYS}}^{\text{upt}_N} \cdot h_{Q_N}^{\text{PHYS}} \cdot \text{PHYS}}_{\text{uptake}} - \underbrace{f_{\text{PHYS}}^m \cdot \text{PHYS}_N}_{\text{nat. mortality}} \\ &- \underbrace{f_{\text{CIL}}^{g^{\text{PHYS}}} \cdot Q_N^{\text{PHYS}} \cdot \text{CIL}}_{\text{grazing by CIL}} - \underbrace{f_{\text{HNF}}^{g^{\text{PHYS}}} \cdot Q_N^{\text{PHYS}} \cdot \text{HNF}}_{\text{grazing by HNF}} \end{aligned} \quad (\text{A.48})$$

$$\begin{aligned} \frac{d\text{PHYS}_P}{dt} &= \underbrace{f_{\text{PHYS}}^{\text{upt}_P} \cdot h_{Q_P}^{\text{PHYS}} \cdot \text{PHYS}}_{\text{uptake}} - \underbrace{f_{\text{PHYS}}^m \cdot \text{PHYS}_P}_{\text{nat. mortality}} \\ &- \underbrace{f_{\text{CIL}}^{g^{\text{PHYS}}} \cdot Q_P^{\text{PHYS}} \cdot \text{CIL}}_{\text{grazing by CIL}} - \underbrace{f_{\text{HNF}}^{g^{\text{PHYS}}} \cdot Q_P^{\text{PHYS}} \cdot \text{HNF}}_{\text{grazing by HNF}} \end{aligned} \quad (\text{A.49})$$

$$\begin{aligned} \frac{d\text{PHYS}_{\text{CHL}}}{dt} &= \underbrace{f^{\text{Pchl}} \cdot \text{PHYS}}_{\text{chlorophyll synthesis}} - \underbrace{f_{\text{PHYS}}^m \cdot \text{PHYS}_{\text{CHL}}}_{\text{nat. mortality}} - \underbrace{f_{\text{CIL}}^{g^{\text{PHYS}}} \cdot Q_{\text{CHL}}^{\text{PHYS}} \cdot \text{CIL}}_{\text{grazing by CIL}} \\ &- \underbrace{f_{\text{HNF}}^{g^{\text{PHYS}}} \cdot Q_{\text{CHL}}^{\text{PHYS}} \cdot \text{HNF}}_{\text{grazing by HNF}} \end{aligned} \quad (\text{A.50})$$

$$f_{\text{PHYS}}^{\text{upt}_N} = f_{\text{PHYS}}^{\text{upt}_{\text{NO}_3}} + f_{\text{PHYS}}^{\text{upt}_{\text{NH}_4}} + f_{\text{PHYS}}^{\text{upt}_{\text{DON}}} \quad (\text{A.51})$$

$$f_{\text{PHYS}}^{\text{upt}_P} = f_{\text{PHYS}}^{\text{upt}_{\text{PO}_4}} + f_{\text{PHYS}}^{\text{upt}_{\text{DOP}}} \quad (\text{A.52})$$

Dissolved organic matter

$$\begin{aligned}
\frac{d\text{LDOC}}{dt} &= - \underbrace{f_{\text{BAC}}^{\text{uptLDOC}} \cdot \text{BAC}}_{\text{gross uptake by BAC}} + \underbrace{f_{\text{BAC}}^m \cdot \text{BAC}_C}_{\text{BAC nat. mort.}} + \underbrace{f_{\text{BAC}}^{\text{uptLDOC}} \cdot (1 - h_{Q_c}^{\text{BAC}}) \cdot \text{BAC}}_{\text{exudation by BAC}} \quad (\text{A.53}) \\
&+ \underbrace{f_{\text{PHYS}}^m \cdot \text{PHYS}_C}_{\text{PHYS nat. mort.}} + \underbrace{f_{\text{nr}}^{\text{PP}} \cdot (1 - h_{Q_c}^{\text{PHYS}}) \cdot \text{PHYS}}_{\text{exudation by PHYS}} + \underbrace{f_{\text{nr}}^{\text{PP}} \cdot (1 - h_{Q_c}^{\text{PHYL}}) \cdot \text{PHYL}}_{\text{exudation by PHYL}} \\
&+ \underbrace{f_{\text{HNF}}^m \cdot \text{HNF}_C}_{\text{HNF nat. mort.}} + \underbrace{f_{\text{BAC}}^{\text{hydDETS}} \cdot \text{BAC}_C}_{\text{DETS hydrolysis}} \\
&+ \underbrace{(f_{\text{HNF}}^{\text{gPHYS}} \cdot Q_C^{\text{PHYS}} + f_{\text{HNF}}^{\text{gBAC}} \cdot Q_C^{\text{BAC}}) \cdot (1 - h_{Q_c}^{\text{HNF}})}_{\text{DOC release by HNF}} \cdot \text{HNF} \\
&+ \underbrace{(f_{\text{CIL}}^{\text{HNF}} \cdot Q_C^{\text{HNF}} + f_{\text{CIL}}^{\text{gPHYS}} \cdot Q_C^{\text{PHYS}}) \cdot (1 - h_{Q_c}^{\text{CIL}})}_{\text{DOC release by CIL}} \cdot \text{CIL} \\
&+ \underbrace{\varepsilon(1 - \gamma) \cdot (f_Z^{\text{gCIL}} \cdot Q_C^{\text{CIL}} + f_Z^{\text{gHNF}} \cdot Q_C^{\text{HNF}} + f_Z^{\text{gPHYL}} \cdot Q_C^{\text{PHYL}}) \cdot (1 - h_Z^{\text{Z}})}_{\text{DOC release by Z}} \cdot \text{Z}
\end{aligned}$$

$$\frac{d\text{SLDOC}}{dt} = - \underbrace{f_{\text{BAC}}^{\text{uptSLDOC}} \cdot h_{Q_c}^{\text{BAC}} \cdot \text{BAC}}_{\text{net uptake by BAC}} \quad (\text{A.54})$$

$$\begin{aligned}
\frac{d\text{LDON}}{dt} &= - \underbrace{(f_{\text{BAC}}^{\text{uptDON}} - f_{\text{BAC}}^{\text{outDON}}) \cdot \text{BAC}}_{\text{net uptake by BAC}} + \underbrace{f_{\text{BAC}}^{\text{hydDETS}} \cdot \text{BAC}_N}_{\text{DETS hydrolysis}} - \underbrace{f_{\text{PHYS}}^{\text{uptDON}} \cdot h_{Q_N}^{\text{PHYS}} \cdot \text{PHYS}}_{\text{net uptake by PHYS}} \\
&+ \underbrace{f_{\text{BAC}}^m \cdot \text{BAC}_N}_{\text{BAC mortality}} + \underbrace{f_{\text{PHYS}}^m \cdot \text{PHYS}_N}_{\text{PHYS mortality}} + \underbrace{f_{\text{HNF}}^m \cdot \text{HNF}_N}_{\text{HNF mortality}} \quad (\text{A.55}) \\
&+ (1 - \beta) \left[\underbrace{f_Z^{\text{gPHYL}} \cdot Z \cdot Q_N^{\text{PHYL}} + f_Z^{\text{gCIL}} \cdot Z \cdot Q_N^{\text{CIL}} + f_Z^{\text{gHNF}} \cdot Z \cdot Q_N^{\text{HNF}}}_{\text{N flux of Z grazing on PHYL, CIL and HNF redirected to DON}} \right]
\end{aligned}$$

$$\begin{aligned}
\frac{d\text{LDOP}}{dt} &= - \underbrace{(f_{\text{BAC}}^{\text{uptDOP}} - f_{\text{BAC}}^{\text{remDOP}}) \cdot \text{BAC}}_{\text{net uptake by BAC}} + \underbrace{f_{\text{BAC}}^{\text{hydDETS}} \cdot \text{BAC}_P}_{\text{DETS hydrolysis}} - \underbrace{f_{\text{PHYL}}^{\text{uptDOP}} \cdot h_{Q_P}^{\text{PHYL}} \cdot \text{PHYL}}_{\text{net uptake by PHYL}} \\
&- \underbrace{f_{\text{PHYS}}^{\text{uptDOP}} \cdot h_{Q_P}^{\text{PHYS}} \cdot \text{PHYS}}_{\text{net uptake by PHYS}} + \underbrace{f_{\text{BAC}}^m \cdot \text{BAC}_P}_{\text{BAC mortality}} + \underbrace{f_{\text{PHYS}}^m \cdot \text{PHYS}_P}_{\text{PHYS mortality}} + \underbrace{f_{\text{HNF}}^m \cdot \text{HNF}_P}_{\text{HNF mortality}} \\
&+ (1 - \beta) \left[\underbrace{f_Z^{\text{gPHYL}} \cdot Z \cdot Q_P^{\text{PHYL}} + f_Z^{\text{gCIL}} \cdot Z \cdot Q_P^{\text{CIL}} + f_Z^{\text{gHNF}} \cdot Z \cdot Q_P^{\text{HNF}}}_{\text{P flux of Z grazing on PHYL, CIL and HNF redirected to DOP}} \right] \quad (\text{A.56})
\end{aligned}$$

Detrital material

$$\begin{aligned}
\frac{d\text{DETL}_C}{dt} &= \underbrace{f_Z^m \cdot Z_C}_{Z \text{ mort.}} + \underbrace{f_Z^{mq} \cdot Q_C^z \cdot Z^2}_{Z \text{ graz. by higher trophic levels}} + \underbrace{f_{\text{PHYL}}^{mq} \cdot Q_C^{\text{PHYL}} \cdot \text{PHYL}^2}_{\text{PHYL grazing by higher trophic levels}} - \underbrace{f_{\text{BAC}}^{\text{hyd}_{\text{DETL}}} \cdot \text{DETL}_C}_{\text{hydrolysis by BAC}} \\
&+ \underbrace{(1 - \varepsilon)(1 - \gamma) \cdot (f_Z^{g^{\text{CIL}}} \cdot Q_C^{\text{CIL}} + f_Z^{g^{\text{HNF}}} \cdot Q_C^{\text{HNF}} + f_Z^{g^{\text{PHYL}}} \cdot Q_C^{\text{PHYL}})}_{\text{faecal pellets released by Z}} \cdot (1 - h_{Q_C^z}) \cdot Z \\
&+ \underbrace{\gamma \cdot (f_Z^{g^{\text{CIL}}} \cdot Q_C^{\text{CIL}} + f_Z^{g^{\text{HNF}}} \cdot Q_C^{\text{HNF}} + f_Z^{g^{\text{PHYL}}} \cdot Q_C^{\text{PHYL}})}_{\text{sloppy feeding released by Z}} \cdot Z \tag{A.57}
\end{aligned}$$

$$\begin{aligned}
\frac{d\text{DETS}_C}{dt} &= - \underbrace{\beta_3 \cdot f_Z^{g_{\text{JUV}}^{\text{SPOC}}} \cdot Z}_{\text{grazing during juvenile stages}} + \underbrace{f_{\text{BAC}}^{\text{hyd}_{\text{DETL}}} \cdot \text{DETL}_C}_{\text{DETL}_C \text{ hydrolysis by BAC}} - \underbrace{f_{\text{BAC}}^{\text{hyd}_{\text{DETS}}} \cdot \text{DETS}_C}_{\text{DETS}_C \text{ hydrolysis by BAC}} \\
&+ \underbrace{f_{\text{CIL}}^m \cdot \text{CIL}_C}_{\text{CIL mort.}} + \underbrace{f_{\text{PHYL}}^m \cdot \text{PHYL}_C}_{\text{PHYL mort.}} \tag{A.58}
\end{aligned}$$

$$\begin{aligned}
\frac{d\text{DETL}_N}{dt} &= \underbrace{f_{\text{PHYL}}^{mq} \cdot Q_N^{\text{PHYL}} \cdot \text{PHYL}^2}_{\text{PHYL grazing by higher trophic levels}} + \underbrace{\beta f_Z^{g^{\text{PHYL}}} \cdot Z \cdot Q_N^{\text{PHYL}}}_{\text{N flux of Z grazing on PHYL redirected to DETL}} - \underbrace{f_{\text{BAC}}^{\text{hyd}_{\text{DETL}}} \cdot \text{DETL}_N}_{\text{hydrolysis by BAC}} \tag{A.59}
\end{aligned}$$

$$\begin{aligned}
\frac{d\text{DETS}_N}{dt} &= \underbrace{f_{\text{CIL}}^m \cdot \text{CIL}_N}_{\text{CIL mort.}} + \underbrace{f_{\text{PHYL}}^m \cdot \text{PHYL}_N}_{\text{PHYL mort.}} + \underbrace{\beta (f_Z^{g^{\text{CIL}}} Z \cdot Q_N^{\text{CIL}} + f_Z^{g^{\text{HNF}}} Z \cdot Q_N^{\text{HNF}})}_{\text{N flux of Z grazing on CIL and HNF redirected to DETS}} \\
&+ \underbrace{\beta_1 f_Z^{g_{\text{JUV}}^{\text{SPON}}} Z \cdot \frac{Q_N^{\text{CIL}}}{Q_C^{\text{CIL}}}}_{\text{grazing by Z during juvenile stages}} + \underbrace{\beta_2 f_Z^{g_{\text{JUV}}^{\text{SPON}}} Z \cdot \frac{Q_N^{\text{HNF}}}{Q_C^{\text{HNF}}}}_{\text{grazing by Z during juv. stages}} + \underbrace{f_{\text{BAC}}^{\text{hyd}_{\text{DETL}}} \cdot \text{DETL}_N}_{\text{DETL}_N \text{ hydroly. by BAC}} \\
&- \underbrace{f_{\text{BAC}}^{\text{hyd}_{\text{DETS}}} \cdot \text{DETS}_N}_{\text{DETS}_N \text{ hydrolysis by BAC}} \tag{A.60}
\end{aligned}$$

$$\begin{aligned}
\frac{d\text{DETL}_P}{dt} &= \underbrace{f_{\text{PHYL}}^{mq} \cdot Q_P^{\text{PHYL}} \cdot \text{PHYL}^2}_{\text{PHYL grazing by higher trop. levels}} + \underbrace{\beta f_Z^{g^{\text{PHYL}}} \cdot Z \cdot Q_P^{\text{PHYL}}}_{\text{P flux of Z grazing on PHYL redirected to DETL}} \\
&- \underbrace{f_{\text{BAC}}^{\text{hyd}_{\text{DETL}}} \cdot \text{DETL}_P}_{\text{hydrolysis by BAC}} \tag{A.61}
\end{aligned}$$

$$\begin{aligned}
\frac{d\text{DETS}_P}{dt} &= \underbrace{f_{\text{CIL}}^m \cdot \text{CIL}_P}_{\text{CIL mort.}} + \underbrace{f_{\text{PHYL}}^m \cdot \text{PHYL}_P}_{\text{PHYL mort.}} + \underbrace{\beta (f_Z^{g^{\text{CIL}}} Z \cdot Q_P^{\text{CIL}} + f_Z^{g^{\text{HNF}}} Z \cdot Q_P^{\text{HNF}})}_{\text{P flux of Z grazing on CIL and HNF redirected to DETS}} \\
&+ \underbrace{\beta_1 f_Z^{g_{\text{JUV}}^{\text{DETS}_P}} Z \cdot \frac{Q_P^{\text{CIL}}}{Q_C^{\text{CIL}}}}_{\text{graz. during juv. stages}} + \underbrace{\beta_2 f_Z^{g_{\text{JUV}}^{\text{DETS}_P}} Z \cdot \frac{Q_P^{\text{HNF}}}{Q_C^{\text{HNF}}}}_{\text{graz. during juv. stages}} + \underbrace{f_{\text{BAC}}^{\text{hyd}_{\text{DETL}}} \cdot \text{DETL}_P}_{\text{DETL}_P \text{ hydrolysis}} \\
&- \underbrace{f_{\text{BAC}}^{\text{hyd}_{\text{DETS}}} \cdot \text{DETS}_P}_{\text{DETS}_P \text{ hydrolysis}} \tag{A.62}
\end{aligned}$$

Nutrients

$$\begin{aligned}
\frac{d\text{NH}_4}{dt} = & - \underbrace{f_{\text{PHYS}}^{\text{upt}_{\text{NH}_4}} \cdot h_{Q_N}^{\text{PHYS}} \cdot \text{PHYS}}_{\text{net uptake by PHYS}} - \underbrace{f_{\text{PHYL}}^{\text{upt}_{\text{NH}_4}} \cdot h_{Q_N}^{\text{PHYL}} \cdot \text{PHYL}}_{\text{net uptake by PHYL}} & (\text{A.63}) \\
& - \underbrace{f_{\text{BAC}}^{\text{upt}_{\text{NH}_4}} \cdot \text{BAC} \cdot h_{Q_N}^{\text{BAC}}}_{\text{net uptake by BAC}} + \underbrace{f_{\text{BAC}}^{\text{rem}_{\text{DON}}} \cdot \text{BAC}}_{\text{mineralization by BAC}} \\
& + \underbrace{(f_{\text{CIL}}^{g^{\text{BAC}}} \cdot Q_N^{\text{BAC}} + f_{\text{CIL}}^{g^{\text{HNF}}} \cdot Q_N^{\text{HNF}} + f_{\text{CIL}}^{g^{\text{PHYS}}} \cdot Q_N^{\text{PHYS}}) \cdot \text{CIL} \cdot (1 - h_{Q_N}^{\text{CIL}})}_{\text{excretion by CIL}} \\
& + \underbrace{(f_{\text{HNF}}^{g^{\text{PHYS}}} \cdot Q_N^{\text{PHYS}} + f_{\text{HNF}}^{g^{\text{BAC}}} \cdot Q_N^{\text{BAC}}) \cdot \text{HNF} \cdot (1 - h_{Q_N}^{\text{HNF}})}_{\text{excretion by HNF}} - \underbrace{f_{\text{NH}_4}^{\text{nit}} \cdot \text{NH}_4}_{\text{nitrification}}
\end{aligned}$$

$$\begin{aligned}
\frac{d\text{NO}_3}{dt} = & - \underbrace{f_{\text{PHYL}}^{\text{upt}_{\text{NO}_3}} \cdot h_{Q_N}^{\text{PHYL}} \cdot \text{PHYL}}_{\text{net uptake by PHYL}} - \underbrace{f_{\text{PHYS}}^{\text{upt}_{\text{NO}_3}} \cdot h_{Q_N}^{\text{PHYS}} \cdot \text{PHYS}}_{\text{net uptake by PHYS}} - \underbrace{f_{\text{BAC}}^{\text{upt}_{\text{NO}_3}} \cdot h_{Q_N}^{\text{BAC}} \cdot \text{BAC}}_{\text{net uptake by BAC}} \\
& + \underbrace{f_{\text{NH}_4}^{\text{nitrif}} \cdot \text{NH}_4}_{\text{nitrification}} & (\text{A.64})
\end{aligned}$$

$$\begin{aligned}
\frac{d\text{PO}_4}{dt} = & - \underbrace{f_{\text{PHYL}}^{\text{upt}_{\text{PO}_4}} \cdot h_{Q_P}^{\text{PHYL}} \cdot \text{PHYL}}_{\text{net uptake by PHYL}} - \underbrace{f_{\text{PHYS}}^{\text{upt}_{\text{PO}_4}} \cdot h_{Q_P}^{\text{PHYS}} \cdot \text{PHYS}}_{\text{net uptake by PHYS}} & (\text{A.65}) \\
& - \underbrace{f_{\text{BAC}}^{\text{upt}_{\text{PO}_4}} \cdot \text{BAC} \cdot h_{Q_P}^{\text{BAC}}}_{\text{net uptake by BAC}} + \underbrace{f_{\text{BAC}}^{\text{rem}_{\text{DOP}}} \cdot \text{BAC}}_{\text{mineralization by BAC}} \\
& + \underbrace{(f_{\text{CIL}}^{g^{\text{BAC}}} \cdot Q_P^{\text{BAC}} + f_{\text{CIL}}^{g^{\text{HNF}}} \cdot Q_P^{\text{HNF}} + f_{\text{CIL}}^{g^{\text{PHYS}}} \cdot Q_P^{\text{PHYS}}) \cdot (1 - h_{Q_P}^{\text{CIL}}) \cdot \text{CIL}}_{\text{excretion by CIL}} \\
& + \underbrace{(f_{\text{HNF}}^{g^{\text{PHYS}}} \cdot Q_P^{\text{PHYS}} + f_{\text{HNF}}^{g^{\text{BAC}}} \cdot Q_P^{\text{BAC}}) \cdot (1 - h_{Q_P}^{\text{HNF}}) \cdot \text{HNF}}_{\text{excretion by HNF}}
\end{aligned}$$